Frequency-Dependent Criteria for Mitigating Effects of Transmission Line Terminated with Linear Loads

BY

NIKHIL KUMAR
B.S., Delhi College Of Engineering, India, 2011

THESIS

Submitted in partial fulfillment of the requirements
For the degree of Master of Science in Electrical and Computer Engineering
At the Graduate College of the
University Of Illinois at Chicago, 2015

Chicago, Illinois

Defense Committee:

Dr. Sudip. K. Mazumder, Chair and Advisor
Dr. Vahe Caliskan
Dr. Sabri Centikunt, Department of Mechanical and Industrial Engineering

This thesis is dedicated to my parents who have always provided their support and encouragement along with endless love for me

ACKNOWLEDGMENTS

This material is based upon the work supported by the National Science Foundation under grant No. 1239118.

Firstly, I would like to express sincere thanks to my advisor Dr. Sudip.K.Mazumder for his unmatched support and encouragement during my graduate years without whom I would not have gotten this far. I also appreciate my advisory committee, Dr. Vahe Caliskan and Dr. Sabri Centikunt for their valuable guidance and comments on my research.

Secondly, I want to acknowledge my family members, especially my mother, Saroj Gupta, for her endless love and care for me. My father, Govind Gupta, who has always supported me in every form throughout my life. My younger brother, Varun Gupta, for being there for our parents always during my absence and his affectionate support at all times.

Finally, I would like to thank my fellow colleagues and dear friends, Ankit Gupta and Harshit Soni, for their invariable support and motivation during my research. I would like to extend thanks to my lab-mates Alireza Mojab, Siamak Mehrnami and Hossein Riazmontezar for their encouragement and humor. In addition, I would like to thank my roommate Rohit Nathani for all the memorable moments we shared during the past couple of years living in Chicago.

NK

CONTRIBUTION OF AUTHORS

Chapter 1 is a literature review that places my dissertation in the context of the larger field and highlights the significance of my research problem. A part of the chapter 2 and 3 represents an unpublished manuscript, (A. Gupta, N. Kumar, and S. Mazumder, "High-Frequency Power Distribution in the Presence of Transmission-Line Effect."submitted for review in IEEE Trans. Power Electronics.") for which I was the second author. Ankit Gupta assisted me in writing the manuscript and getting the experimental results as provided in chapter 3. My research mentor Dr.Sudip.K.Mazumder also contributed to the writing of the manuscipt.

TABLE OF CONTENTS

CHAPTER PAGE

LIST OF TABLES

TABLE PAGE

LIST OF FIGURES

FIGURE PAGE

LIST OF FIGURES (CONTINUED)

FIGURE PAGE

LIST OF FIGURES (CONTINUED)

FIGURE PAGE

SUMMARY

Rapid advancements in power semiconductor devices has accelerated the growth of power electronics system to the point that, high frequency distributed power system (HFDPS) has become a practical reality, provided that transmission-line effects are mitigated. Benefits of HFDPS can be realized in applications ranging from nanogrids, smart-buildings, all-electric warships and microgrids. However, its usage has been limited to applications where the choice of path does not affect the power quality or the signal integrity due to transmission-line effects a signal encounters as it propagates through the transmission medium. In the past, researchers have shown different approaches to mitigate the transmission-line effects by using impedance matching networks/adjusting transmission-line length or employing active compensation along the transmission line to ensure signal integrity. In this Dissertation, a frequency-dependent criteria is developed for a HFDPS, feeding linear load(s), which can mitigate transmission-line effects under periodic conditions and facilitate high frequency power transfer through long transmission-line lengths. Selection of transmission frequency is of critical importance while designing a HFDPS; otherwise it aggravates the system performance by introducing distortion and offsetting signal integrity in form of ringing, crosstalk, reflection and ground bounce. In addition, the applicability of the developed criteria has been explored for single-input single-output (SISO), single-input multi-output (SIMO) and multi-input multi-output (MIMO) topologies along with its validation using simulation and experimental results.

CHAPTER I. INTRODUCTION

1.1. Motivation and Objectives

Ever increasing environmental concerns and energy demand have paved the pathway for research and development of more efficient and reliable power generation and distribution systems. In recent times, distributed power system (DPS) has emerged as a solution to tackle such problems [1]. Contrary to the conventional power system where, power generation is centralized and long transmission networks are used for energy distribution; DPS is decentralized, modular, more flexible and suitable across a range of applications including electric power, mechanical power and propulsion [2]**.** In a DPS the total power required by a load can be supplied by a single source or spatially distributed multiple sources connected in various network architectures, usually with a main aim to bring the power processing unit closer to the load centers and increase system efficiency and reliability.

Figure 1 illustrates various DPS mechanisms available for transferring power from the distributed sources to the loads. Of these the low frequency ac and dc based DPSs, as illustrated in Figures 1a and 1b are the conventional means of power transfer. In Figure 1(a), a DC DPS requires an active front end and back end power electronics system (PES) for power conversion and active and reactive power control, thus making it complex and costlier**.** Also, galvanic isolation has always been a challenge in a dc DPS whereas, a low frequency power transfer or an ac DPS as shown in Figure 1(b) requires a HF link, which act as an interface for power conversion from dc to ac (i.e. DC-HFAC-DC-AC), in turn increasing the number of power conversion stages and decreasing the efficiency of the overall system. Furthermore, a low frequency power transfer suffers from poor dynamic performance in the event of sudden change in power requirement by

the loads or failure as well as lower power density. However, for applications including microgrids, telecommunication, electric vehicles, aerospace, defense, lighting, and computer systems, a high frequency distributed power system (HFDPS) as illustrated in Figures. 1(c) and 1(d), provide plurality of advantages over the conventional DPS including high efficiency, fast system dynamics, enhanced reliability, and high power density. Consequently, HFDPS has emerged as an alternative to a conventional ac and dc DPS.

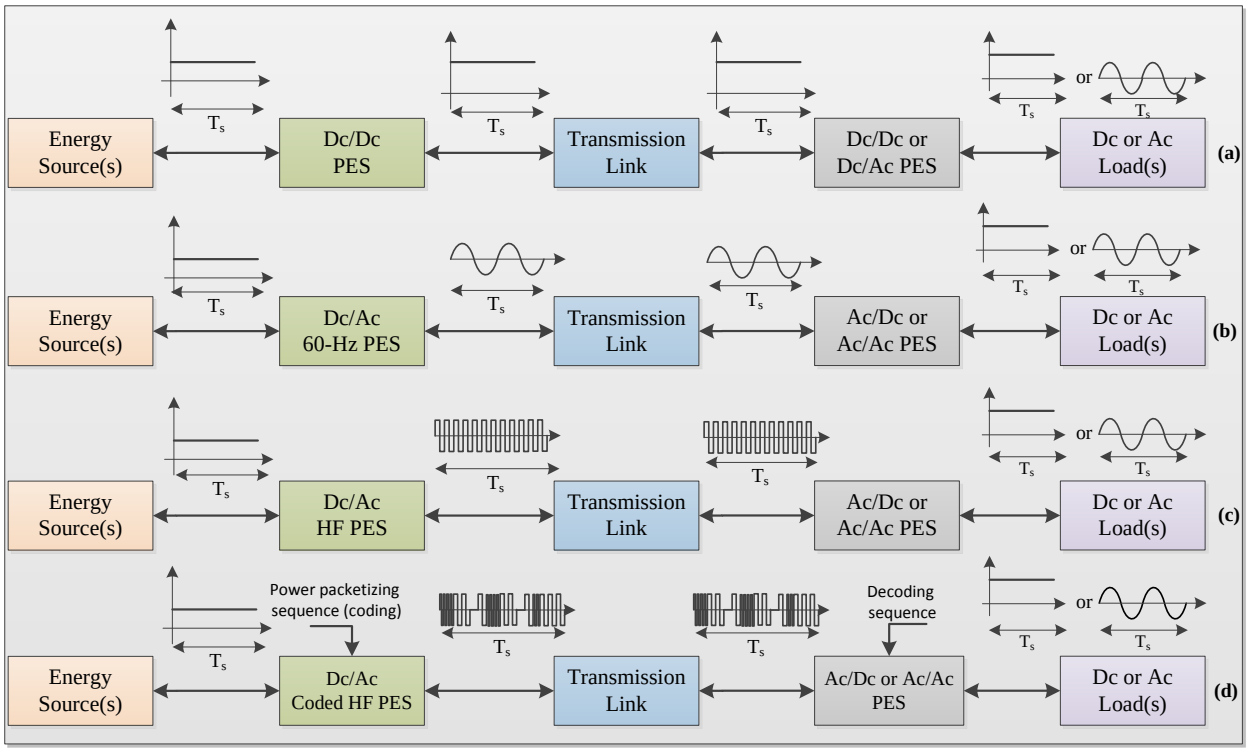

Figure 1. Architecture of (a) dc, (b) ac, and (c), (d) HFDPSs. The difference between (c) and (d) pertains to how the HF power signals are transmitted

Coded HFDPS architecture as shown in Figure 1(d) differs from a traditional HFDPS in terms of power delivery methodology, power management, power signal signature and in its control and communication mechanism. A traditional HFDPS delivers power to the assigned loads using a HF link in a continuous manner, as in a low frequency or a dc DPS. On the contrary, a coded HFDPS

shown in Figure 1(d) emulates the internet by feeding tailor made (with encoded data) power in discrete form to assigned loads in a discontinuous manner using front end PES. This may partially de-escalate the requirement of load-end PES by reducing the number of power conversion stages thereby increasing the system efficiency along with decreasing cost and complexity.

One of the key feature of coded HFDPS is that, it incorporates need based power transfer, i.e. demand of power will address its availability. Since power will be available only for the duration in which demand is generated, utilization of transmission link can be optimized as well as losses in PES can be minimized. In this manner, for a given time cycle, power requirement by the loads can be addressed more proficiently, and in an event driven fashion guided by dynamic-priority assigned to each load by the load energy management system. The assigned dynamic priority will be based on the severity, amount and frequency of power required by the loads [3]**.**

A traditional HFDPS and a coded HFDPS no doubt, have superiority over a dc or an ac DPS in terms of efficiency, associated cost and reliability, but their implementation have been primarily limited to small systems where dimensions do not affect the overall integrity of the system.

In recent times, escalation in demand of higher power density, improved power quality and system efficiency have been majorly addressed by the advancement in manufacturing technology of semiconductor devices which are capable of switching at high frequencies**.** But, such high frequency switching gives rise to unwanted electromagnetic interference (EMI) and excite multi-mode oscillations in parasitic couplings in form of transmission-line (TL) effects [2], which in turn offsets the integrity of the signal. .

When the wavelength of signal being transmitted through a medium is comparable to the physical length of the medium itself, the TL effects comes into play. Figure 2 captures the variation in length of TL (with parameters tabulated in table I) at which onset of TL effect occurs as a function of frequency of wave transmission [4].

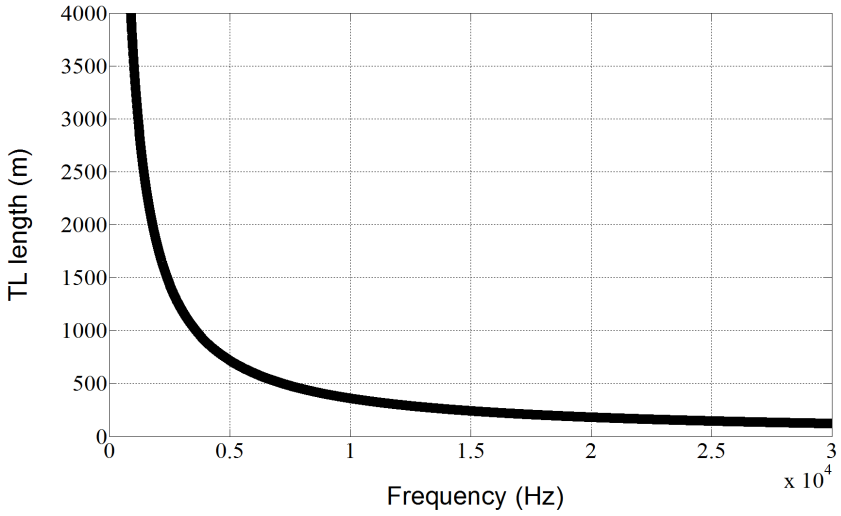

Figure 2. Illustration of the length of a given TL, for a given frequency of wave propagation, at which the TL effect onsets. The parameters of the TL are captured in table I.

Table 1. Parameters of a TL used for the simulation

Quantity	Value
Characteristic impedance	50 Ω
Inductance	0.1968 μH/m
Capacitance	80.688 pF/m
Velocity of propagation	84%
Delay	3.96 ns/m
Dc resistance	1.7384 m

The specific objectives of this dissertation are the following:

- To analyze effects of transmission-line terminated with linear loads in the event of high frequency power transfer and to provide a methodology for the mitigation of these effects such that signal integrity is ensured.
- To extend the developed methodology from single-input single-output HFDPS network topologies to single-input multi-output and multi-input multi-output HFDPS network topologies.

1.2. Literature Review

In this section, literature concerning HFDPS for an electrical power system (EPS) for space applications, electrical vehicle, telecommunication, computer and commercial electronics system is reviewed. In addition, effects of TL in HFDPS as well as steps taken towards its mitigation in motor drives, induction pumps, induction heating system and on chip interconnections will be summarized.

One of the earliest attempts on a HFDPS was undertaken by NASA Lewis Research Centre in 1983, for the space station freedom program [5]. The aim was to design an efficient, low cost and highly reliable electrical power system (EPS) for a permanent orbiting space facility. The space facility had to be solar powered with output power of 75 kW. A detailed comparison was done among 150 Vdc, 440 Vac-400 Hz, 440 Vac-20 kHz. Results outlined in [5] confirmed that, the 20 kHz power management and distribution model was more efficient, cheaper and lighter than the dc distributed power system and 400 Hz alternative, available in that period. The main challenge to the proposed high frequency scheme was to design a low inductive power cable such

that, the cross-talks during the load variations and worst case voltage variations can be handled with reduced skin effect losses.

Another HFDPS for a low power application employing a hybrid resonant inverter topology was proposed by Jain and Tanju in [6]. The topology was developed with an aim to meet the high efficiency, tight output voltage regulation and low total harmonic distortion for the proposed international space station mobile servicing system (MSS). The inverter generated a quasi-square voltage at the output of inverter which was filtered out by doubly tuned series and parallel resonant networks, tuned at inverter operating frequency. Results in [6] demonstrated the inverter output voltage stiffness within 2 percent over varying load demand.

Sood and Lipo [7] also proposed a system configuration based on a 20 kHz single phase voltage link for distributed power systems for space application required by NASA Lewis Research Centre.. The high frequency link interface converters utilized an area comparison pulse density modulated (PDM) scheme in order to synthesize wide variety of signals. Results outlined in [7] displayed the synthesized sinusoidal as well as dc current in single or three phase form with very low harmonic distortion. Also, the proposed configuration allowed flexibility in voltage levels, without employing bulky magnetic components together with fast response and reduced acoustic noise; and provides high degree of uniformity and ease of implementation.

Jain [8] proposed a hybrid high frequency (100 kHz or higher) ac power distribution architecture for application in space and telecommunication systems. A novel HFDPS which has the advantages of both high frequency constant voltage and high frequency constant current distribution system was presented. The proposed configuration in [8] was operated in three modes; a) Power transfer mode (contactless power transfer through magnetic coupling), b) No load mode (current limiting by offering very high impedance) and c) Short circuit mode (fuse less protection)

in order to achieve connector-less power transfer, sinusoidal current and voltage distribution with low EMI and high overall system efficiency from full load to ¼ load.

Antaloae in [9] investigated the feasibility of high frequency ac (HFAC) for powering auxiliary loads in automotive electric vehicles. The study was focused to evaluate the practicality of replacing dc/ac inverters with 100 V, 50 kHz HFAC/ac networks for high torque ac machines. The present 14 V dc bus had several shortcomings which included expensive and heavy wiring harness, oscillation of dc bus voltage and high failure rate of connectors. Results in [9] displayed the predominance of HFAC/ac system over dc/ac system in terms of reduction in copper loss due to lower voltage harmonics. Also, it indicated potential copper weight savings as well as system compactness due to high frequency operation along-with high transmission efficiency.

Bose and Kankam in [10] proposed and then demonstrated the viability of high frequency AC (HFAC) for propulsion DPS in next generation hybrid electric vehicle. A comparative study between the traditional dc DPS and the single phase HFAC system was outlined. The study established the superiority of HFAC system in terms of switching loss elimination, higher reliability, less EMI, absence of acoustic noise and less dv/dt stress on machine insulation. In addition, HFAC proved to be more economical and efficient than dc in terms of overall component sizing calculations.

S. Chakraborty [11] studied a high frequency (500 Hz) link AC microgrid which integrated renewable energy sources including photovoltaic solar arrays, fuel cell and battery. In [11], to compensate for the reactive power, load current harmonics and voltage distortions, a p-q theory based active filters called unified power quality conditioner (UPQC) and unified power line conditioner (UPLC) were used to address the issue of power quality and power flow. A distributed intelligent energy management system (DIEMS) was implemented to optimize the operating cost

of the microgrid. Results in [11] displayed an improvement in power quality in terms of unity power factor with minimum voltage distortions, resulting in sinusoidal load voltage.

S. Lourdes, S. Y. Ng and P.C.K Luk in [12] discussed the advantages of an alternative power grid by proposing a systematic framework to facilitate quantitative evaluation of the characteristics of a HFAC DPS. A set of eleven performance parameters including power factor, line regulation, THD as well as transients specifications had been used to formulate the system performance index such that assessment and comparison can be established between HFAC DPS and other DPS.

References [5]-[14] has demonstrated the benefits of power transfer at high frequency which includes reduction in size of bulky transformers, inductors and capacitors employed in low frequency (utility) system. The ease of galvanic isolation using compact high frequency transformer and reduction in power conversion steps, together with the prospects of significant savings in component count and system integration has proved its superiority over a dc and ac DPS. High frequency operation also improves system dynamic performance and reduces acoustic noise.

But, HFDPS application has been majorly limited to printed circuit board (PCB) implementations or applications where choice of path does not affect the power quality or the signal integrity. As mentioned in 1.1, high switching frequencies, give rise to TL effects which aggravates the system performance by introducing distortion and offsetting signal integrity in form of ringing, crosstalk, reflection and ground bounce.

For instance, in high speed IC’s which generates signals of rise and fall time in order of few ns, that the device capacitance combined with parasitic inductance of the interconnects of a gate drive circuit behave as a transmission line. These IC’s may be used to generate gate drive signals

for a power semiconductor devices in a converter and consists of voltage and currents of different frequencies propagating down the transmission line. Although, fundamental frequency may be much lower to cause any TL effects but the frequencies which contribute to the rapid rise and fall times of a gate signal are much higher and can result in debilitating effects like voltage overshoot, undershoot, false triggering of the gate and loss of signal properties. Thus, these parasitics of the circuit can no more be analyzed as a lumped element but as a distributed parameters where transmission line techniques must be employed.

One way of mitigating the TL effects involves insertion of impedance matching network using quarter wave transformers, filters and series or parallel stubs (L sections) thus ensuring no signal integrity issues [15][16][17][18][19][20]. Another method is to provide active compensation or power factor correction techniques along the TL, which ensures signal integrity for wide range of frequencies [21]**.** While the former is limited to the systems where layout of the system can easily be altered, the latter leads to an increase in the associated cost and complexity of the compensated system.

The transmission line effects had been experienced and analyzed by many researchers in the past, in applications which includes inverter fed PWM motor drives for induction motors, the on chip interconnections or traces on a PCB board, voltage source inverter fed high frequency induction heating systems, on board microcontrollers employed in hybrid electric vehicles and high speed data transfer in digital systems [16][18][22]-[25]

Erik persson in [23] investigated the transient effects in application of PWM inverters on a standard squirrel cage induction motor. The motor was subjected to non-sinusoidal wave shapes when supplied from adjustable frequency inverters. It was confirmed that, motor cables behaves as a transmission line for the pulses with rise time greater than the time taken for the pulse to travel

to and fro over cables. Also, high impedance ratio of motor and characteristic impedance of the cables caused full reflection of the voltage pulse at the motor terminals. This reflection in turn ramped up the voltage on the motor terminal, which was hazardous to the motor insulation and caused high turn to turn stress.

David B. Hyypio [24] also investigated the effects of rise-time of PWM waveforms generated by voltage source inverters and cable length on their contribution to destructive corona producing energy due to overshoots caused by reflection at motor terminals. The voltage response at the motor terminals was studied using finite difference model for a 150 ft. cable with rate of change of voltage of 5000 V/microsecond and rise time of 0.1 microsecond. Results in [8] confirmed that, cable length played an important role in determining the corona energy produced by reflection if compared to rise time of inverter output voltage. Also, it was stated that, it is the energy associated with the process of partial discharge that identifies the degree of stress on the motor insulation instead of peak voltage and rise-time of waveforms.

To solve the problem of high current high frequency components due to wiring between a voltage fed type inverter and a LC resonant load circuit for high frequency induction heating system Kawahara [16] developed a power transmission method which utilized the distributed constant line (D.C.L). A $\lambda/4$ distributed constant line (also known as quarter wave transformer) was used in order to increase the high frequency impedance as seen by the inverter hence, suppressing the high frequency currents. To determine its potency, a comparison between a LC lumped constant circuit and the D.C.L was done at high frequencies in the range of MHz. Result in [11] indicated that the waveform of the inverter output current was approximately sinusoidal in nature for both of the arrangements. It was confirmed, that TL effects can be easily cope up by using a flexible coaxial cable as a distributed constant line or by impedance matching.

Dalal [18] proposed a high frequency transmission line transformer (TLT) for DC/DC converters. It utilized cascades of interconnected TL sections made of parallel strips of metal sandwiching the dielectric material on a PCB. It was demonstrated that, an efficient storage and transfer of energy was possible without requiring a core. The filtering effect that inherently exists in TLT's, provides and additional advantage in power converters where high frequency harmonics are inevitably generated due to switching. Also, the electrical isolation was provided by connecting the TLT's in a particular manner.

Deutsch [22] studied the effect of on-chip interconnections of line width in range of 0.45-0.52 μm.The study presented the guidelines for transmission-line effect consideration for accurate delay and crosstalk prediction. The performance limiting parameters such as delay introduced due to capacitive coupling with adjacent interconnections, fast signal transition resulting in higher noise as well as crosstalk for short, medium and long interconnections were highlighted respectively.

On the basis of TL length and the frequency of wave transmission (i.e., the propagation of the source-originated temporal power signal through the spatially-distributed TL) a HFDPS can be broadly classified in two categories: one which encounters TL effects and other, which does not. For HFDPS encountering the TL effects, most of the publications have employed variation in either TL parameters or length of the TL for elimination and mitigation of these effects. Also, they have been limited to SISO or SIMO topology configurations.

1.3. Thesis Outline

This Dissertation primarily focuses on addressing the TL effects encountered during high frequency power transfer. There are 3 chapters in total including introduction.

Chapter II presents a basic introductory theory on TL followed by derivation of its parameters using telegrapher's equation. Consequently, effects of the TL have been realized and an approach for its mitigation using frequency-dependent criteria has been outlined. The developed criteria is then extended to various HFDPS with single input single output (SISO), single input multi output (SIMO) and multi input multi output (MIMO) topologies.

Chapter III provides the experimental results in frequency domain as well as time domain as a validation to support the developed frequency-dependent criteria for each topology discussed in Chapter II. It also includes the simulated parametric variation of input impedance with the parameters of a TL and frequency of wave transmission. Finally, conclusions of this work and suggestions for the future work are exposed.

CHAPTER II. ANALYSIS OF TRANSMISSION-LINE EFFECTS

2.1. Transmission line theory and Telegrapher's wave equations

In this chapter, an introduction to TL and basic telegrapher's equation for a lossy and lossless TL is outlined followed up by detailed discussion on different HFDPS topologies. Also, frequency-dependent criteria is developed by exploiting the periodicity property exhibited by the input impedance as seen by the source followed by a TL terminated with passive linear loads.

A Transmission line (TL) is generally referred to as a system which is capable of guiding TEM (transverse electromagnetic) waves. It can be represented by a pair of conductors carrying signal from a transmitter to receiver. A TL is composed of distributed inductance (L), distributed capacitance (C), distributed resistance (R) and distributed dielectric conductance (G) per unit length. Equivalent circuit model for a lossless TL, excluding dissipative elements (resistance and conductance) is shown in Figure 3. Figure 4 displays a dissipative model of TL.

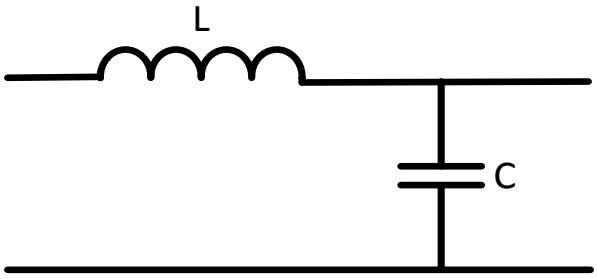

Figure 3. Equivalent circuit model of a lossless TL

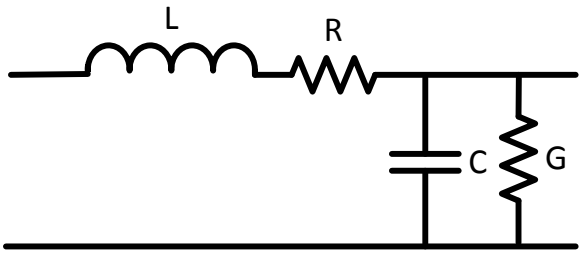

Figure 4. Equivalent circuit model of a lossy TL

Every TL is identified by its characteristic impedance and the speed (velocity of propagation) with which an electrical signal can propagate. Propagation of signal manifests itself into continuous charging and discharging of inductor and capacitor followed by attenuation of the signal. As the signal propagates, it incorporates some delay which depends on the line length and velocity of propagation. The impedance encountered during the charging of the first LC section is the characteristic impedance or instantaneous impedance which is the most important property of a TL.

A common rule of thumb is, that a wire or cable should be treated as a TL, if the physical length of the wire is greater than one tenth of the electrical wavelength of the signal being transmitted.

$$l > \frac{\lambda}{10}$$

where, $$\lambda = \frac{v}{f}$$

Symbol v and f being the velocity of propagation and frequency of wave transmission respectively. Hence, TL behavior becomes more evident as the frequency of signal being transmitted increases. As frequency is increased progressively, in lieu of TL effects a circuit cannot be analyzed using Kirchhoff's laws, but an approach called transmission-line theory.

The series inductance L represents total self-inductance of the two conductors and the shunt capacitance C represents the proximity of the two conductors. The series resistance R is due to the finite conductivity of the individual conductors and shunt conductance G is due to the dielectric loss in the material between the conductors.

Figure 5 depicts an equivalent circuit model for an extremely short section of a TL of length Δz, where Δz is much smaller than the wavelength of the transmitted signal ($\Delta z << \lambda$). The inductance and capacitance in this equivalent circuit provides the time delay and phase shift

lacking in treatment of the TL in a conventional circuit theory [26]**.** By including them, the equivalent lumped parameter circuit segment can be analyzed using Kirchhoff's laws.

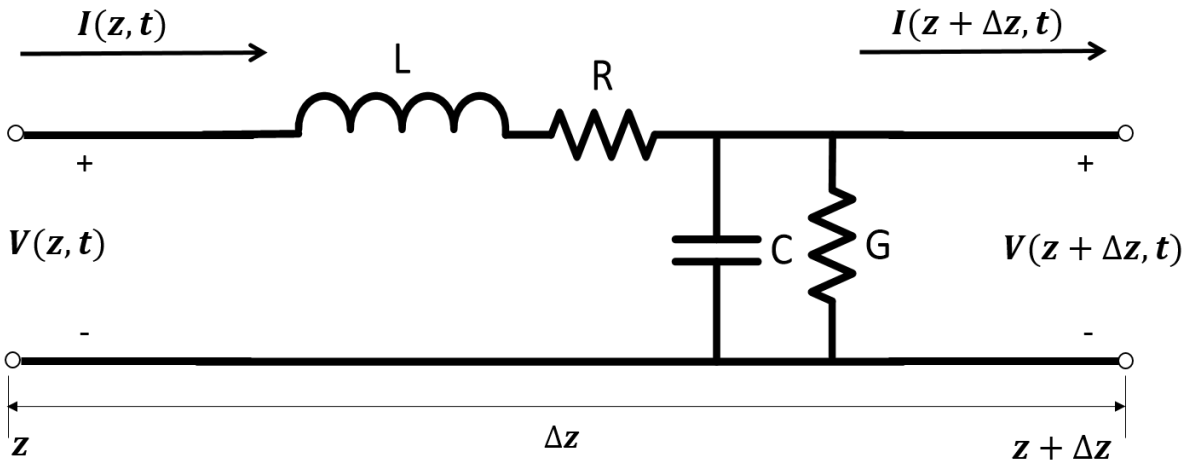

Figure 5. Equivalent circuit model for the short section of a TL

In Figure 5, the quantity $L\Delta z$, $R\Delta z$, $C\Delta z$, $G\Delta z$ represents total series inductance, series resistance, shunt capacitance and shunt conductance of the equivalent circuit.

Applying Kirchhoff voltage law on the circuit displayed in Figure 5 yields,

$$V\ (z+\Delta z,t)\ +\ L\Delta z\frac{\partial I}{\partial t}\ +R\Delta z I(z,t)=V(z,t) \tag{2.1}$$

In the limiting case, when Δz tends to zero, (2.1) can be represented as

$$\frac{\partial V}{\partial z}=\ -L\frac{\partial I}{\partial t}\ -\ RI(z,t) \tag{2.2}$$

Applying Kirchhoff's current law on the circuit in Figure 5 yields,

$$I\ (z+\Delta z,t)\ +\ C\Delta z\frac{\partial V}{\partial t}\ +G\Delta z V(z+\Delta z,t)=I(z,t) \tag{2.3}$$

In limiting case, when Δz tends to zero, (2.3) can be represented as

$$\frac{\partial I}{\partial z} = -C\frac{\partial V}{\partial t} - GV(z,t) \tag{2.4}$$

Equation (2.2) and (2.4) represents time domain form of TL equations, also known as Telegrapher's equations. Partial differentiation of (2.2) and (2.4) w.r.t. ∂z yields,

$$\frac{\partial^2 V}{\partial z^2} = -L\frac{\partial^2 I}{\partial t.\partial z} - R\frac{\partial I(z,t)}{\partial z} \tag{2.5}$$

$$\frac{\partial^2 I}{\partial z^2} = -C\frac{\partial^2 V}{\partial t.\partial z} - G\frac{\partial V(z,t)}{\partial z} \tag{2.6}$$

Substituting expression of $\frac{\partial^2 I}{\partial z^2}$ in (2.5) and $\frac{\partial^2 V}{\partial z^2}$ in (2.6), a hyperbolic partial differential equation is obtained involving only one unknown,

$$\frac{\partial^2 V}{\partial z^2} = LC\frac{\partial^2 V}{\partial t^2} + (GL + RC)\frac{\partial V(z,t)}{\partial t} + GRV(z,t) \tag{2.7}$$

$$\frac{\partial^2 I}{\partial z^2} = LC\frac{\partial^2 I}{\partial t^2} + (GL + RC)\frac{\partial I(z,t)}{\partial t} + GRI(z,t) \tag{2.8}$$

(2.7) and (2.8) represents the homogeneous wave equations with extra terms in V and I and their first derivatives, where second and third term in (2.7) and (2.8) cause signal to disperse and attenuate with time and distance. It should be noted that, if a TL is considered as a lossless ($R = 0, G = 0$) or only slightly lossy (2.7) and (2.8) reduces to

$$\frac{\partial^2 V}{\partial z^2} = LC\frac{\partial^2 V}{\partial t^2} \tag{2.9}$$

$$\frac{\partial^2 I}{\partial z^2} = LC\frac{\partial^2 I}{\partial t^2} \tag{2.10}$$

The general solution for such partial differential equation can be expressed by,

$$V(z,t) = V_1 e^{j(\omega t - \beta z)} + V_2 e^{j(\omega t + \beta z)} \tag{2.11}$$

Where β represents the wavenumber of the TL and is given by,

$$\beta = \omega\sqrt{LC} = \frac{\omega}{v} . \tag{2.12}$$

Symbols ω and v represent angular velocity and velocity of propagation of the signal being transmitted over a TL. Since,

$$v = \lambda f \tag{2.13}$$

wavenumber β can also be expressed in terms of λ by the relationship,

$$\beta = \frac{2\pi}{\lambda} . \tag{2.14}$$

Expression for I can be obtained by substitution of (2.11) in (2.4) (considering a lossless TL)

$$I(z,t) = I_1 e^{j(\omega t - \beta z)} - I_2 e^{j(\omega t + \beta z)} \tag{2.15}$$

Where, $I_1 = \frac{C\omega}{\beta} V_1$ and $I_2 = \frac{C\omega}{\beta} V_2$

Using (2.12) in, $I_1 = \frac{C\omega}{\beta} V_1$ and $I_2 = \frac{C\omega}{\beta} V_2$

$$I_1 = V_1 / \sqrt{\frac{L}{C}} \tag{2.16}$$

$$I_1 = V_2 / \sqrt{\frac{L}{C}} \tag{2.17}$$

Where $\sqrt{L/C}$ represents characteristic impedance of a TL and will be represented by Z_{cl} in upcoming sections and chapters.

The negative sign in $(\omega t - \beta z)$ represents a wave travelling in forward direction i.e. from source to load whereas, positive sign in $(\omega t + \beta z)$ represents a wave travelling in backward

direction i.e. from load to source. Symbols V_1 and I_1 represent amplitude of voltage and current signals of the incidental wave at load-end whereas, V_2 and I_2 represents amplitude voltage and current signals of the reflected wave at load-end. Thus, total voltage and current at any given point on a lossless TL are given by (2.11) and (2.15) respectively.

If a TL is considered as lossy ($R \neq 0, G \neq 0$), general solution of (2.7) and (2.8) looks of the form,

$$V(z,t) = V_1 e^{j(\omega t - \gamma z)} + V_2 e^{j(\omega t + \gamma z)} \tag{2.18}$$

$$I(z.t) = I_1 e^{j(\omega t - \gamma z)} - I_2 e^{j(\omega t + \gamma z)} \tag{2.19}$$

where, γ represents propagation constant of the TL. Substitution of (2.18) and (2.19) in (2.7) and (2.8) yields,

$$\gamma^2 + LC\omega^2 = (LG + RC)j\omega + RG. \tag{2.20}$$

(2.20) can further be rearranged and solved for γ,

$$\gamma = \pm\sqrt{(R + j\omega L)(G + j\omega C)} = \alpha + j\beta \tag{2.21}$$

where, α represents attenuation constant or accounts for the lossy factor of the TL. Thus, total voltage and current for a lossy TL at any point is given by,

$$V(z,t) = V_1 e^{-\alpha z + j(\omega t - \beta z)} + V_2 e^{\alpha z + j(\omega t + \beta z)} \tag{2.22}$$

$$I(z,t) = I_1 e^{-\alpha z + j(\omega t - \beta z)} + I e^{\alpha z + j(\omega t + \beta z)} . \tag{2.23}$$

Characteristic impedance Z_{cl} for a lossy TL can be calculated by substituting (2.18) in (2.4) and its expression is given by,

$$Z_{cl} = \sqrt{\frac{(R + j\omega L)}{G + j\omega C}} \tag{2.24}$$

For the sinusoidal steady state conditions, with cosine based phasors (2.11), (2.15), (2.22) and (2.23) simplifies to

$$V(z) = V_1 e^{-j\beta z} + V_2 e^{j\beta z} \tag{2.25}$$

$$I(z) = I_1 e^{j\beta z} - I_2 e^{j\beta z} \tag{2.26}$$

$$V(z,t) = V_1 e^{-\alpha z - j\beta z} + V_2 e^{\alpha z + j\beta z} \tag{2.27}$$

$$I(z,t) = I_1 e^{-\alpha z - j\beta z} + I e^{\alpha z + j\beta z} \tag{2.28}$$

These equations will be used as a basis for outlining the importance of input impedance as seen by the source followed by a TL terminated with passive linear loads and its applicability to various HFDPS topologies with TL effects into consideration.

2.2. Analysis of Different HFDPS Topologies

Figure 6 illustrates a simplified representation of a generalized HFDPS. Essentially, the HFDPS provides a pathway for power transfer between energy source(s) and application load(s) over a TL network that may have a singular/plural path-invariant/path-varying TL(s). Such a HFDPS may have multiple topological manifestations including SISO, SIMO, and MIMO configurations. Further, the load in Figure 6 may not be monolithic load. Given these, initial elaboration, an analyses for three distinctly HFDPS topologies leading to outline of corresponding frequency-dependent criteria that mitigate distortion of power signal under periodic condition is carried out. For each of the cases, initially a specific analysis is described, followed up by an outline on how it is extended to address variations of each of the architectures.

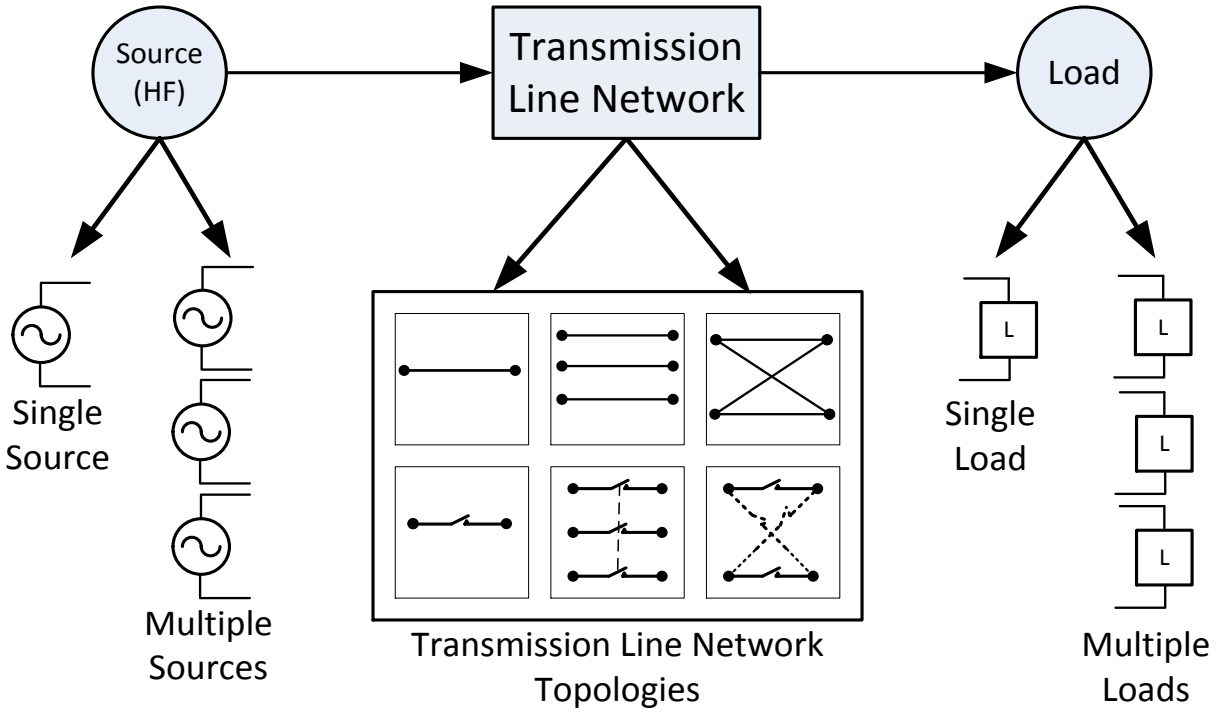

Figure 6. Illustration of a simplified representation of a generalized HFDPS, which provides a power-transfer pathway between energy source(s) and application load(s) (which may/may not be monolithic) over a network that may have a singular/plural path.

2.2.1. HFDPS with SISO Topology

Figure 7 shows a HFDPS with a pathway marked in bold illustrating a SISO power transfer originating at a single source (S_1) and terminating at a single load (L_1) with an impedance of Z_{L1} by closing the source and load-side switches u_{S1} and u_{L1}, respectively. It is noted that, a SISO realization for the HFDPS can be obtained in several other ways by linking any one source to any one load with/without a preceding TL. For all of these scenarios, the scenario-centric analysis carried out next is applicable with small variations that will be outlined at the end of the analysis. As mentioned earlier, we assume that the source S_1 is connected to load L_1 (with an impedance of Z_{L1}) via a lossless TL network with a characteristic impedance of Z_{cl} and a length of l. Further, let Z_{in} represent the impedance at the input (or source-end) of the SISO topology as illustrated in Figure 7.

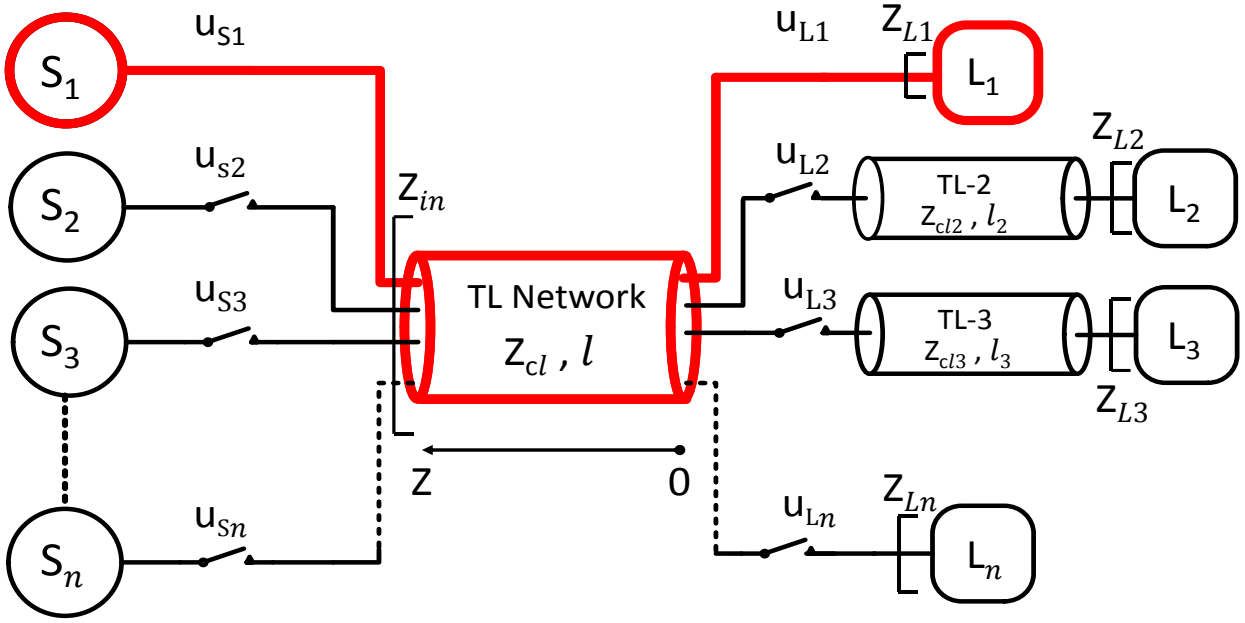

Figure 7. Illustration of a SISO power transfer for a HFDPS. The TL network can be configured to realize multiple other SISO realizations by connecting any one source to any one load with/without a preceding TL.

The input impedance ($Z_{in}(z)$) at a distance z from the load is represented by $Z_{in}(z)$ = V(z)/I(z), where V(z) and I(z) are the voltage and current of the TL network at a distance z from the load, respectively.

When a voltage ($V_1 e^{-j\beta z}$) is incident on a TL, the accompanying current in the transient state is solely determined by the characteristic impedance of the TL. If the load impedance (Z_L) is not equal to the characteristic impedance (Z_{cl}), a reflected wave is generated at the load end leading to a distortion in the received signal [27] **.**The total voltage and current seen at any distance z from the load on the TL is given by the following expression

$$V(z) = V_1 e^{-j\beta z} + V_2 e^{j\beta z} \tag{2.29}$$

$$I(z) = \frac{V_1}{Z_{cl}} e^{-j\beta z} + \frac{V_2}{Z_{cl}} e^{j\beta z} \tag{2.30}$$

Where, $V_1 e^{-j\beta z}$ and $V_2 e^{j\beta z}$ represent the incident and reflected voltage waves, respectively. Symbol β represents the wavenumber of the TL given by $2\,\pi\,/\lambda$ (i.e.$\beta = 2\pi/\lambda$), where λ is the length of the wave being transmitted through the TL. At $z = 0$

$$Z_{in}(0) = Z_{\mathrm{L1}} = \frac{V(0)}{I(0)} = \frac{V_1 + \mathrm{V}_2}{\frac{V_1}{Z_{cl}} - \frac{\mathrm{V}_2}{Z_{cl}}} \,. \tag{2.31}$$

Bilinear transformation [22] on (2.31) yields the following:

$$\frac{V_1}{\mathrm{V}_2} = \frac{Z_{\mathrm{L1}} - Z_{cl}}{Z_{\mathrm{L1}} + Z_{cl}} = \Gamma_L \tag{2.32}$$

Where, Γ_L represents the reflection coefficient at the load-end. Replacing V_2 with Γ_L in (2.29) and (2.30), one obtains

$$V(z) = \mathrm{V}_1 e^{-j\beta z} + \Gamma_L \mathrm{V}_1 e^{+j\beta z} \tag{2.33}$$

$$I(z) = \frac{\mathrm{V}_1}{Z_{cl}} e^{-j\beta z} - \Gamma_L \frac{\mathrm{V}_1}{Z_{cl}} e^{+j\beta z} \tag{2.34}$$

Thus, at a distance z from the load, the observed input impedance is given by the following expression:

$$Z_{in}(\mathrm{z}) = \frac{V(z)}{I(z)} = Z_{cl} \left[\frac{e^{-j\beta z} + \Gamma_L e^{+j\beta z}}{e^{-j\beta z} - \Gamma_L e^{+j\beta z}}\right] \tag{2.35}$$

Substituting Γ_L from (2.32) into (2.35), we obtain the following after simplification of the resultant expression:

$$Z_{in}(z) = Z_{cl}\frac{Z_{\mathrm{L1}} - jZ_{cl}\tan(\beta z)}{Z_{cl} - jZ_{\mathrm{L1}}\tan(\beta z)}.$$

(2.36)

By substituting z = - l in (2.36), the expression for Z_{in} (input impedance reflected at the source end of the SISO topology) is found to be the following:

$$Z_{in} = Z_{cl}\frac{Z_{\mathrm{L1}} + jZ_{cl}\tan(\beta l)}{Z_{cl} + jZ_{\mathrm{L1}}\tan(\beta l)}$$

(2.37)

It is important to note that, in (2.35) substitution of $\beta l = n\pi$ (where n is an integer) always yields:

$$Z_{in} = Z_{\mathrm{L1}} \tag{2.38a}$$

Also, if we substitute $\beta l = m\pi/2$ (where m is an odd integer) in (2.37), it will always yield

$$Z_{in} = {Z_{cl}}^2/Z_{\mathrm{L1}} \tag{2.38b}$$

The TL length which satisfies (2.38a) is obtained by equating $\beta = 2\pi/\lambda$ and $\beta = n\pi/l$ thereby yielding the following relationship:

$$l = \frac{n\lambda}{2}. \tag{2.39a}$$

Also, the TL length which satisfies (2.38b) is obtained by equating $\beta = 2\pi/\lambda$ and $\beta = m\pi/2l$ thereby yielding the following relationship:

$$l = \frac{m\lambda}{4} = \frac{mv}{4\mathrm{f}}. \tag{2.39b}$$

Alternately, (2.38a) is also satisfied if the frequency of the wave transmission is so selected such that $l = \frac{n\lambda}{2} = \frac{nv}{2f}$ (where v and f are the velocity of wave propagation and frequency of wave transmission, respectively, in the TL and $\lambda = v/f$ [27]) yielding

$$f = \frac{nv}{2l}. \tag{2.39c}$$

For any other frequency of wave transmission that does not satisfy (2.39c), (2.38a) is not satisfied as well. Instead, Z_{in} could exhibit resistive or reactive impedance for the same load [4]**.** For instance, if one considers, that S_1 has to transfer power to L_2 which is preceded by an additional TL (TL-2), the same procedure can be followed in two steps. First, a set of frequencies have to be determined which emulates (2.39c) using parameters of TL-2 and then a subset of the obtained frequency set is to be establish using the parameters of the TL network for which (2.39c) is satisfied. Similar analysis can also be applied if air is chosen as the transmission medium instead of a waveguide. The difference will appear in the set or subset of frequencies obtained using (2.39c) as v assume a different value for air.

2.2.1.1. Analysis of characteristics of a Lossless TL terminated with passive linear loads

The accompanying section outlines the expression for the input impedance as seen by the source when TL is terminated with passive linear loads which includes reactive (inductor, capacitor and resistor) and resistive loads. Also, subsequent figures illustrates the dependency of input impedance on frequency of wave transmission. The expression for normalized input impedance (ς_{in}) has been calculated for SISO topology as shown in Figure 7 using (2.37). Table 2 illustrates the applicability of (2.39c) to reactive and resistive loads such that (2.38a) is satisfied.

Table 2. Input impedance expression for reactive and resistive loads

For Reactive loads	For Resistive loads
$Z_{\mathrm{L1}} = R + jX_L - jX_c$	$Z_{\mathrm{L1}} = R$
Normalizing impedances w.r.t Z_{cl}	
$\varsigma_{\mathrm{L1}} = r + jx_L - jx_c$	$\varsigma_{\mathrm{L1}} = r$
Substituting ς_L in (2.35)	
$\varsigma_{in} = \dfrac{r + j(x_L - x_c + \tan\beta l)}{(1 - x_L \tan\beta l + x_c \tan\beta l) + j\mathrm{r}\tan\beta l}$	$\varsigma_{in} = \dfrac{r + j\tan\beta l}{1 + j\mathrm{r}\tan\beta l}$
Magnitude of $\varsigma(z)$	
$\lvert\varsigma(z)\rvert = \sqrt{\dfrac{r^2 + (x_L - x_c + \tan\beta l)^2}{(1 - x_L\tan\beta l + x_c\tan\beta l)^2 + (r\tan\beta l)^2}}$	$\lvert\varsigma(z)\rvert = \sqrt{\dfrac{r^2 + (\tan\beta l)^2}{1 + (r\tan\beta l)^2}}$
Phase of $\varsigma(z)$	
$\phi = \tan^{-1}\left(\dfrac{(x_L - x_c + \tan\beta l)(1 - x_L\tan\beta l + x_c\tan\beta l) - r^2\tan\beta l}{r + r\,(\tan\beta l)^2}\right)$	$\phi = \tan^{-1}\left(\dfrac{(1 - r^2)\tan\beta l}{r + r\,(\tan\beta l)^2}\right)$
At $l = \frac{n\lambda}{2} = \frac{nv}{2f}$ Where v and f are propagation velocity and source frequency respectively	
$\lvert\varsigma(z)\rvert = \sqrt{r^2 + (x_L - x_c)^2}$	$\lvert\varsigma(z)\rvert = r$
$\phi = \tan^{-1}\left(\dfrac{x_L - x_c}{r}\right)$	$\phi = 0$
De-normalizing the impedances using $Z_{in} = \varsigma_{in}\,(Z_{cl})$	
$Z_{in} = \sqrt{R^2 + (X_L - X_c)^2}$	$Z_{in} = R$

A lossless TL of 50 Ω characteristic impedance and length of 12.543 m was chosen for simulation purpose. Figure 8 displays an instance for which load impedance (Z_{L1}) is equal to characteristic impedance (Z_{cl}) of the TL. It is seen that the input impedance magnitude and phase is independent of frequency, enabling the load to receive distortion-less signal with high signal integrity.

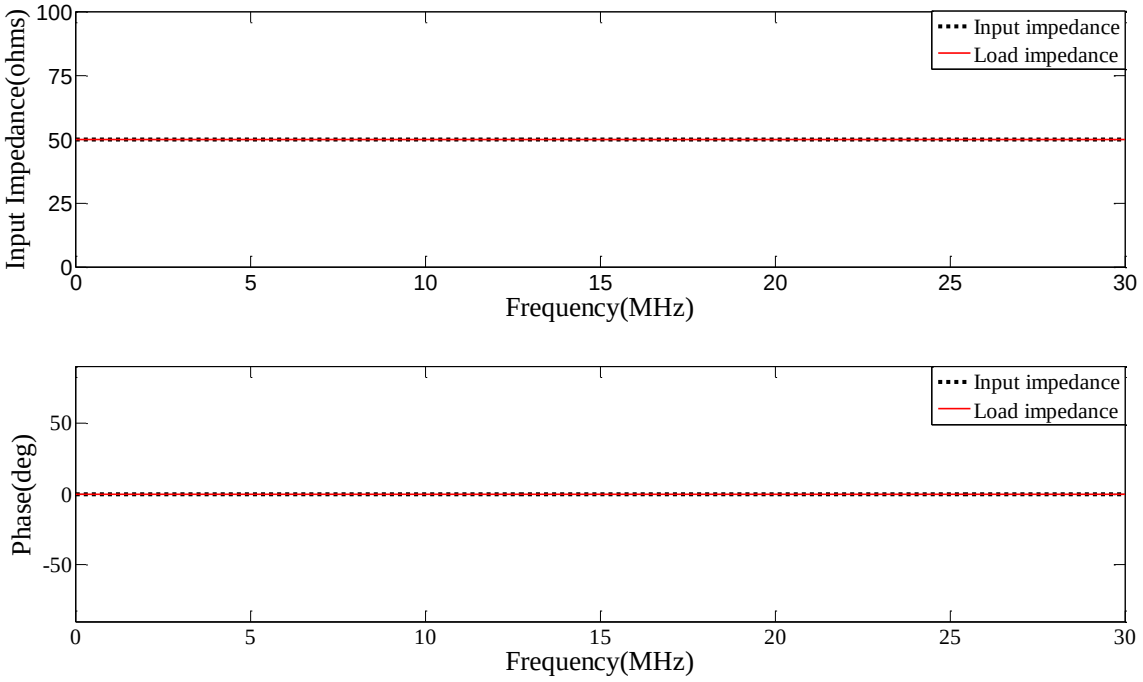

Figure 8. Variation in input impedance with frequency of wave transmission for matched load impedance of 50 Ω

Figure 9 and 10 illustrates the variation of input impedance with frequency for load impedance (Z_{L1}) not equal to characteristic impedance (Z_{cl}) of the TL. It is seen that, only at particular frequencies the input impedance (Z_{in}) is equal to load impedance (Z_{L1}) in steady state. Also, the frequencies at which (2.38a) is satisfied, lies at integral multiple of 10 MHz, which corresponds to frequency obtained using $f = \frac{v}{2l}$. It should be noted, that input impedance is resistive at integral

multiples of 5 MHz and its value is given by 25 Ω using (2.38b), which corresponds to frequencies obtained using $f = \frac{v}{4l}$.

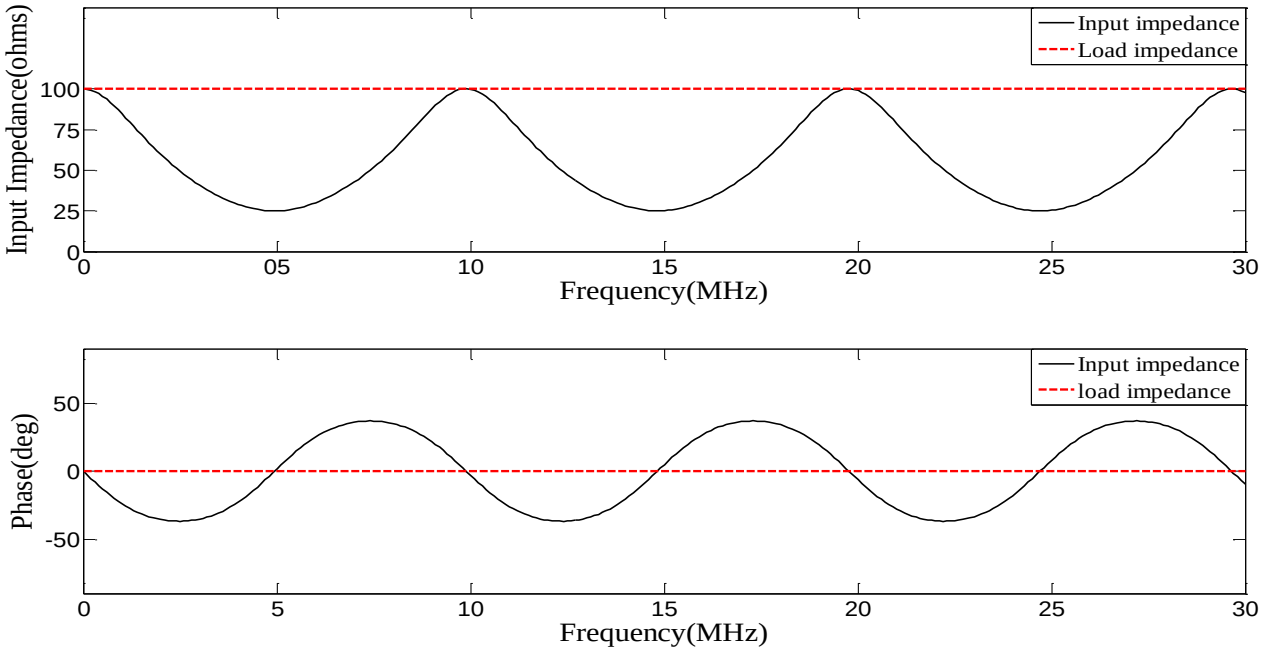

Figure 9. Variation in input impedance with frequency of wave transmission for resistive load impedance of 100 Ω

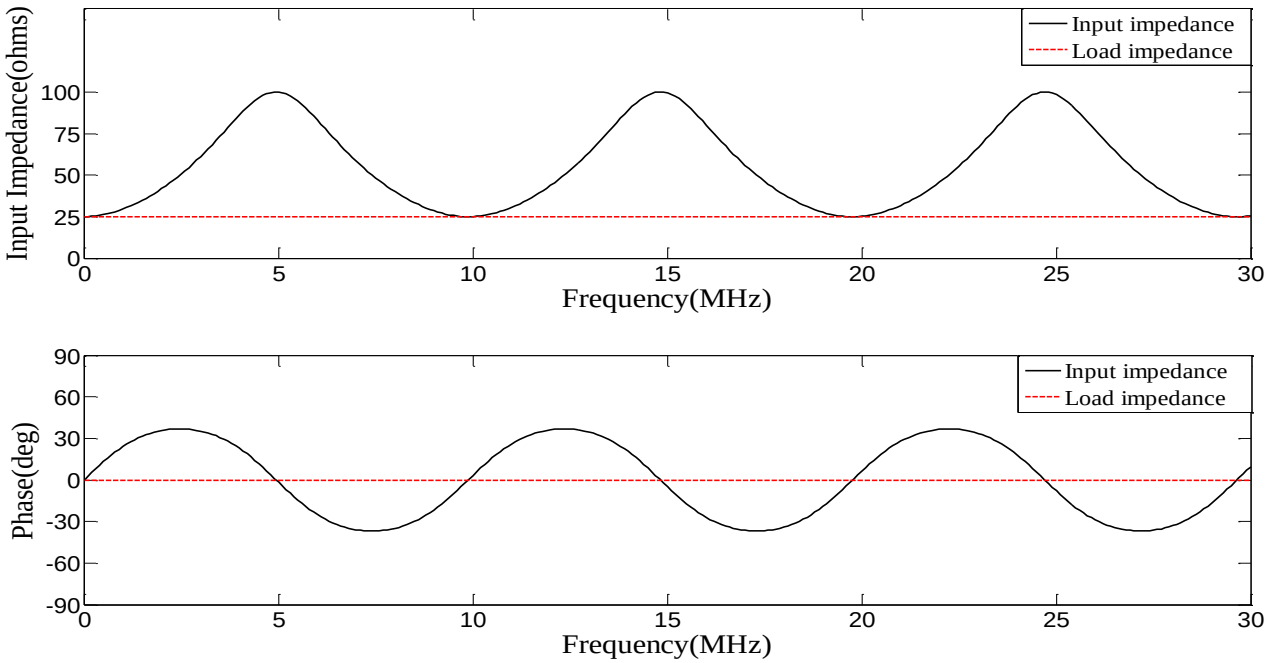

Figure 10. Variation in input impedance with frequency of wave transmission for resistive load impedance of 25 Ω.

Figure 11 -13 represents the variation of input impedance with frequency of wave transmission for reactive (R-L, R-C, R-L-C) loads. It illustrates that, (2.38a) is satisfied at the intersection of input impedance and load impedance. The peaks and troughs in input impedance magnitude curve can be realized as a transition from inductive to capacitive behavior and vice-versa respectively.

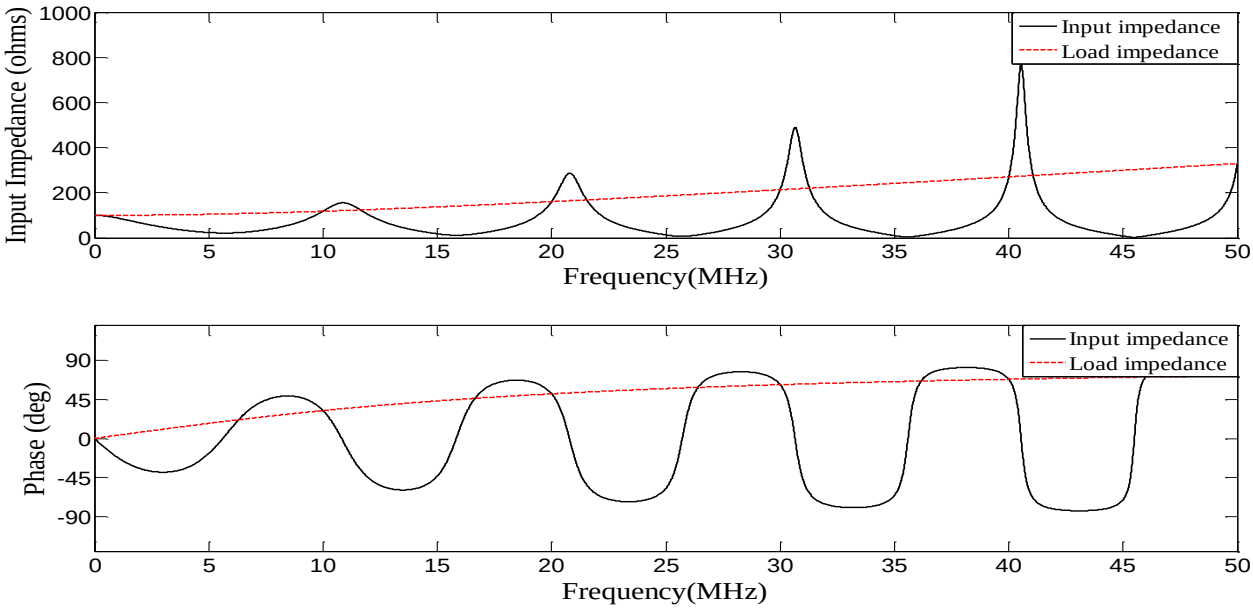

Figure 11. Variation in input impedance with frequency of wave transmission for reactive (R-L) load

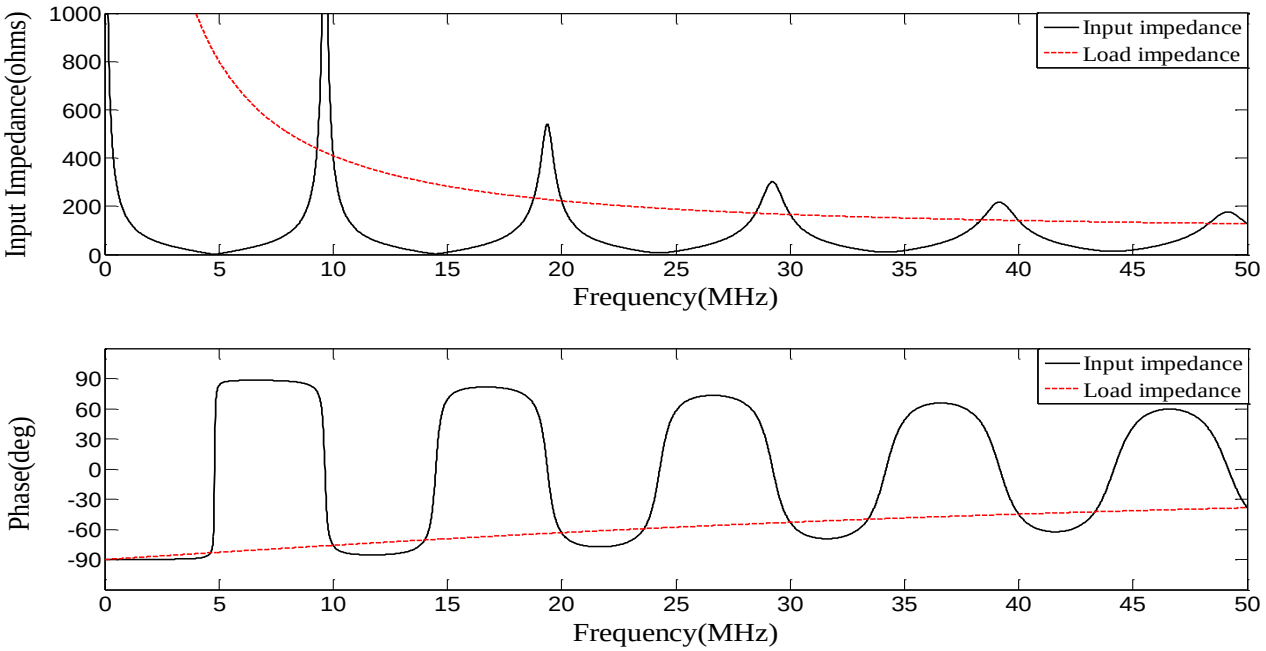

Figure 12. Variation in input impedance with frequency of wave transmission for reactive (R-C) loads

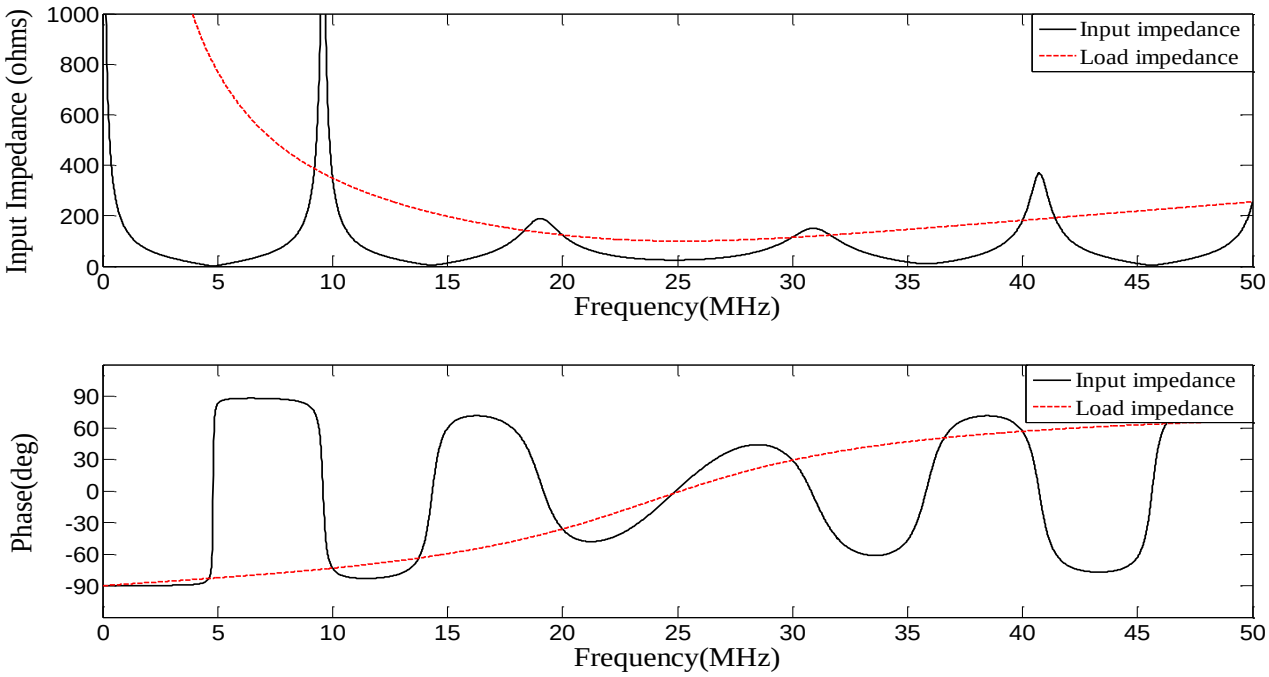

Figure 13. Variation in input impedance with frequency of wave transmission for R-L-C load

Figures 14 and 15 represents variation of the input impedance with frequency of wave transmission for pure inductive and capacitive loads without any leakage resistance. Again (2.38a)

is satisfied at the intersection of load impedance and input impedance. The peaks in the magnitude curve represents resonance condition developed due to parallel combination of inductance and capacitance of line resulting in an open circuit. The troughs in the curve represents resonance condition developed due to series combination of inductance and capacitance of the line resulting a short circuit. It can be inferred, that the peaks and troughs refers to a singularity (limiting condition) at which phase of input impedance approaches zero which is unattainable.

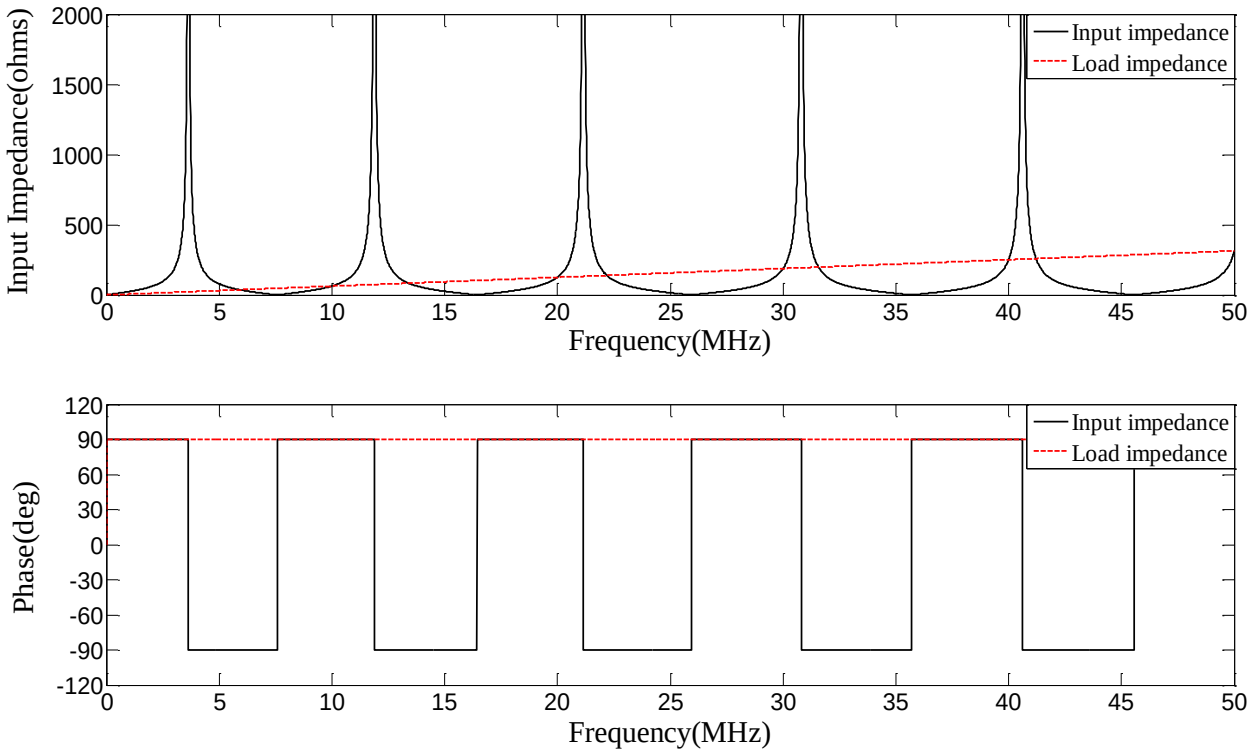

Figure 14.Variation in input impedance with frequency of wave transmission for inductive (L) load.

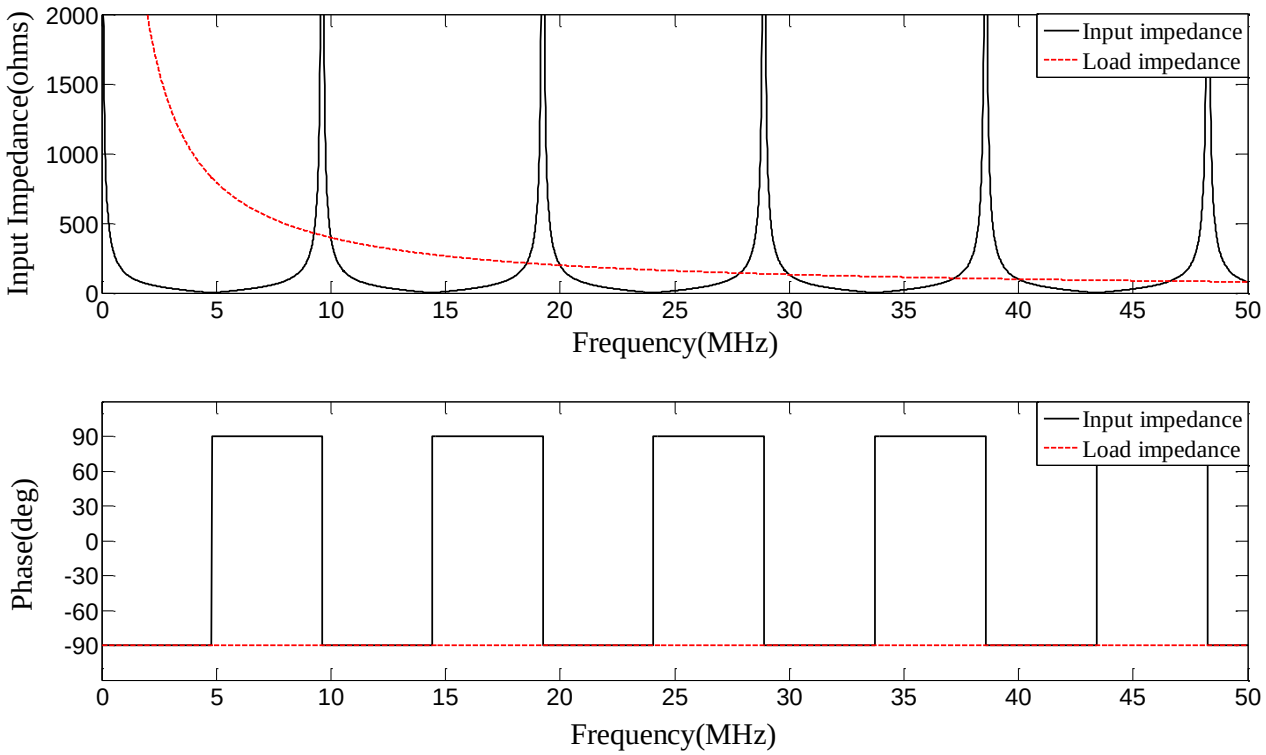

Figure 15. Variation in input impedance for frequency of wave transmission for capacitive (C) load.

2.2.2. HFDPS with SIMO Topology

Figure 16 displays a SIMO power transfer marked in bold, where a single source (S_1) feeds multiple loads ($L_1$and L_2) placed at different locations. There are number of ways of realizing SIMO topology by switching any single source (S_1, S_2 … or S_n) and multiple loads (Z_{L1},Z_{L2} …Z_{Ln}) in either manner by closing $u_{s1,}$, $u_{s2,}$…or $u_{sn,}$ and $u_{L1,}$ $u_{L2,}$ … $u_{Ln,}$ according to the load requirements. In Figure 16, load L_2 is connected via TL network and TL-2 of same characteristic impedance yet different length (l, l_2), whereas load L_1 is located at the junction of TL network and TL-2. Assuming the characteristic impedance of the TLs are equal.

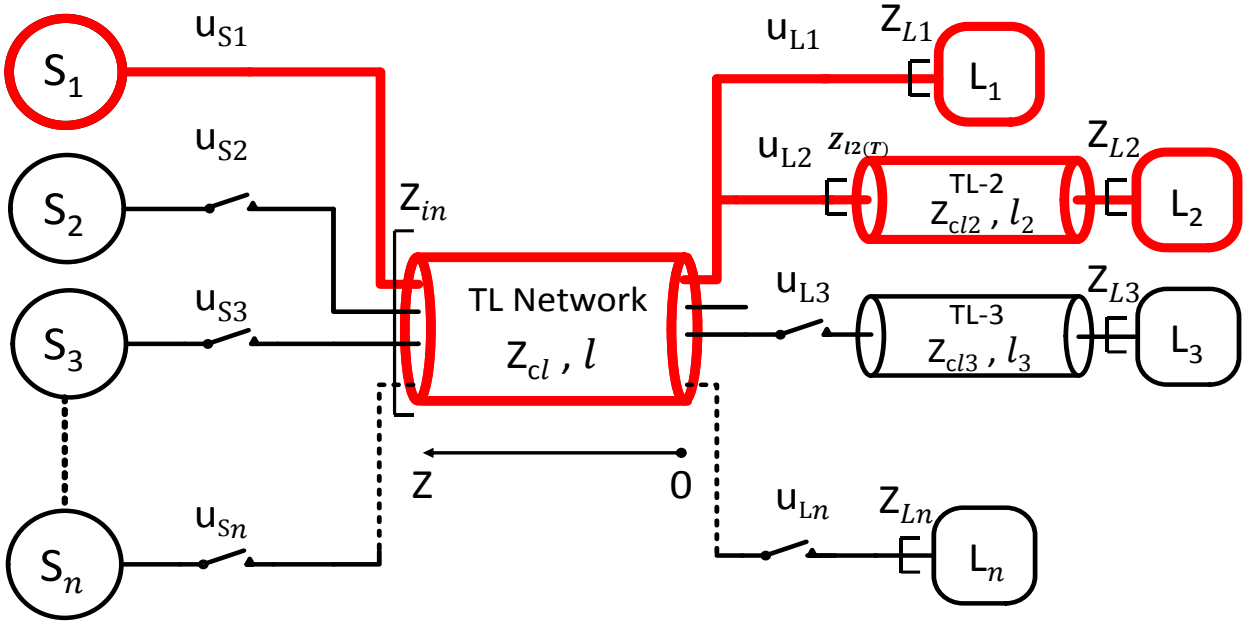

Figure 16. SIMO topology having an intermediate load Z_{L1} at the junction of TL network and TL of length l and l_2. TL network is configured in such a manner that, a single source at its input is connected to two loads at its output.

Using (2.35), the impedance $Z_{l2(T)}$ at the input terminal of TL-2 is given by:

$$Z_{l2(T)} = Z_{cl}\frac{Z_{L2} + jZ_{cl}\tan(\beta l_2)}{Z_{cl} + jZ_{L2}\tan(\beta l_2)} \tag{2.40}$$

This impedance appears in parallel with Z_{L1} and the equivalent impedance will be given by:

$$Z_T = Z_{l2(T)} \parallel Z_{L1} \tag{2.41}$$

Similarly, for TL network (Z_{cl} , l) Z_T will act as the load impedance. Plugging the value of Z_T in (2.37), the input impedance at the source is given by:

$$Z_{in} = Z_0 \left[\frac{\left\{ \frac{(Z_{L1}Z_{L2}Z_0 + jZ_{L1}{Z_0}^2 \tan(\beta l_2))}{Z_0(Z_{L1} + Z_{L2}) + j\tan(\beta l_2)(Z_{L1}Z_{L2} + {Z_0}^2)} \right\} + jZ_0 \tan(\beta l)}{j\left\{ \frac{(Z_{L1}Z_{L2}Z_0 + jZ_{L1}{Z_0}^2 \tan(\beta l_2))\tan(\beta l)}{Z_0(Z_{L1} + Z_{L2}) + j\tan(\beta l_2)({Z_0}^2 + Z_{L1}Z_{L2})} \right\} + Z_0} \right]$$

(2.42)

It is important to note that, substitution of $\beta l = n\pi$ and $\beta l_2 = m\pi$ (where m is an integer) in (2.42) yields

$$Z_{in} = \frac{Z_{L1}Z_{L2}}{Z_{L1} + Z_{L2}}$$

(2.43)

Similar to subsection 2.2.1, for a given l and l_2, if the frequency of wave transmission is selected following $f = \frac{nv}{2l} = \frac{mv}{2l_2}$, (2.43), which represents the impedance matching condition, is satisfied. The latter ensures signal integrity by mitigating the TL effects between S_1 and L_1 and L_2. For any other frequency of wave transmission, (2.43) is not satisfied. Figure 17 illustrates the variation of input impedance with frequency of wave transmission for the marked topology in Figure 16. Two loads of impedance $Z_{L1} = Z_{L2} = 100\ \Omega$ were selected. The length of both TL network (l) and TL-2 (l_2) were chosen to be equal to 12.75 m. Also, the characteristic impedance of TL and TL-2 were considered to be same.

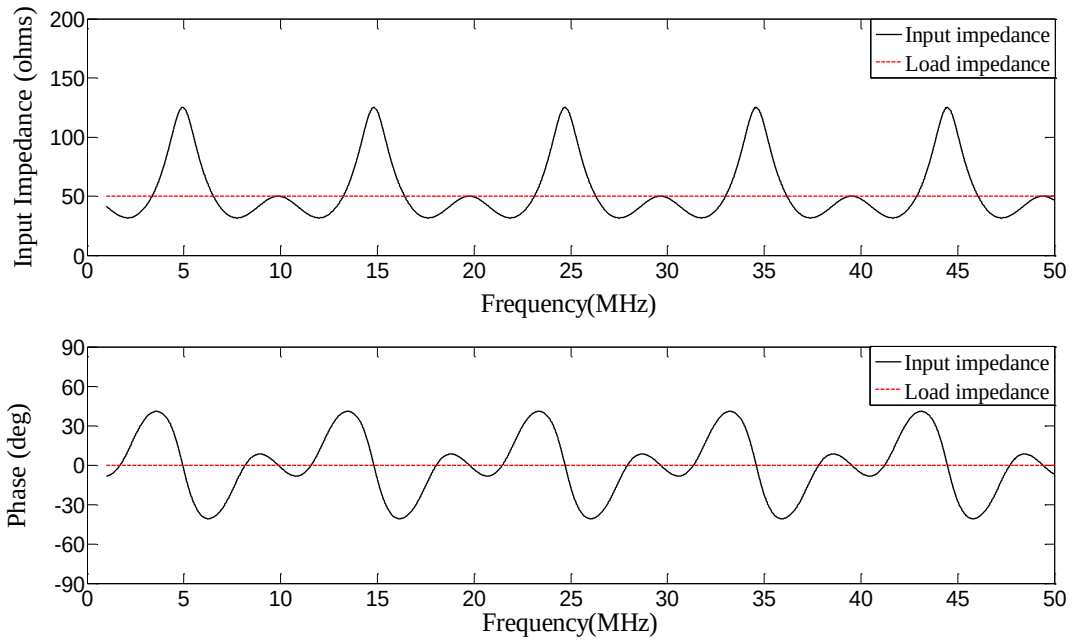

Figure 17. Variation in input impedance with frequency of wave transmission for SIMO topology (Z_{L1}=100 Ω and Z_{L2}=100 Ω and $l = l_1$=12.75 m

It was concluded in subsection 2.2.2 that, frequencies which satisfies $f = \frac{nv}{2l} = \frac{mv}{2l_2}$, for the given length of TL, the input impedance at those frequencies is expressed by (2.43) which would have been the case, if no TL effects were present. It can be observed that (2.43) is satisfied only at integral multiples of 10 MHz and its value is given by 50 Ω with 0 phase. Also, at odd integral multiples of 5 MHz, which pertains to the set obtained by following (2.39b), input impedance is resistive in nature but its value is given by 125 Ω which follows from (2.38b). This can be realized from Figure 16, as when the length of the TL is exactly equal to or odd integral multiple of one-quarter of the wavelength of the opearting frequency of a system given by (2.39b), the input impedance at the source end becomes dual of the impedance with which it is terminated. Hence, a TL for those particular frequencies is sometimes dictated by the term " Quarter-wave impedacne transmformer". In Figure 17, at 5 MHz and its integral multiples, TL-2 acts as a quarter-wave tranformer for Load L_2 and its value at the junction of TL network and TL-2 is given by $Z_{l2(T)}$=

25 Ω using, (2.38b). This impedance apperas in parallel with load L_1 and the value of equivalent impedance is found to be Z_T= 20 Ω. Furthermore, the TL netowrk also acts as quarter-wave transformer at 5 MHz and its integral multiples. Thus, the input impedance at the input port of TL network is given by Z_{in}=125 Ω. Figure 18 displays input impedacne variation in terms of a reactive load and resistive load.

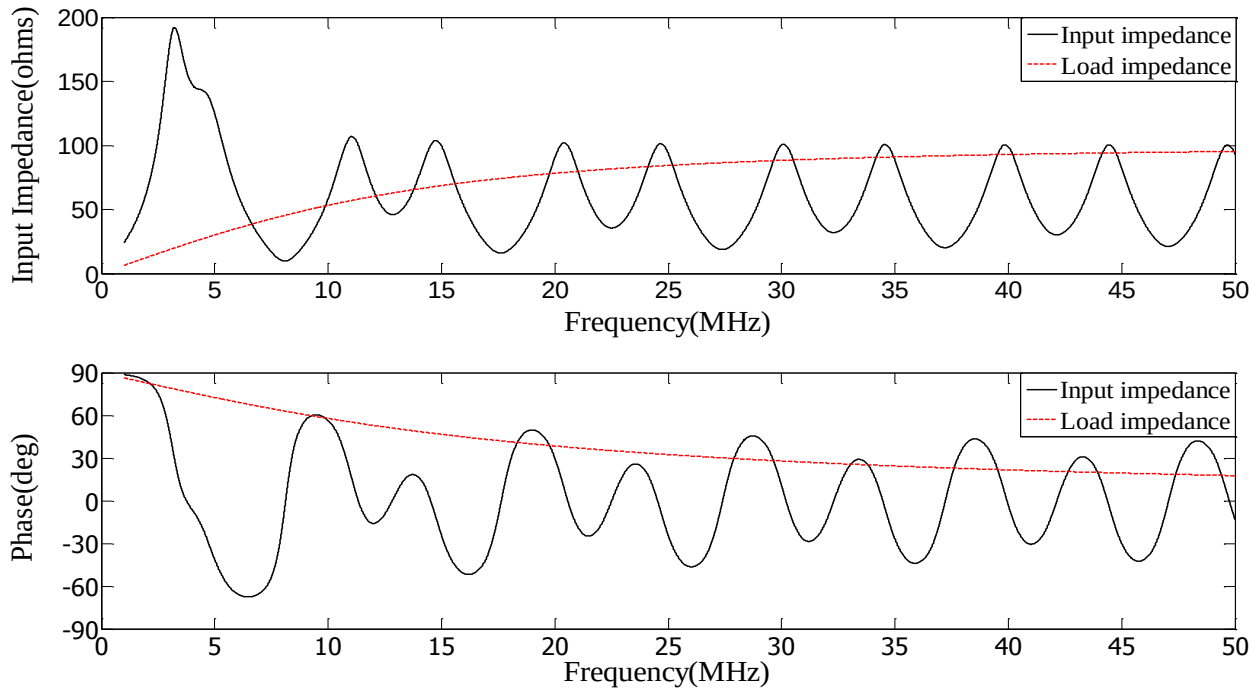

Figure 18. Variation in input impedance with frequency of wave transmission for SIMO topology (Z_{L1}= 1μH and Z_{L2}=100 Ω and $l = l_1$=12.75 m

Load L_1, L_2 were chosen to be an inductive load and resistive load respectively. Other parameters including length and characteristic impedance of the TL network and TL-2 were considered to be same. It is observed, that (2.43) both in magnitude and phase is satisfied only at integral multiples of 10 MHz, given by the points located at the intersection of load impedance and input impedance curve. Here load impedance is chosen to be a parallel combination of Loads L_1 and L_2 as if there is no TL between source (S_1) and the loads (L_1, L_2).

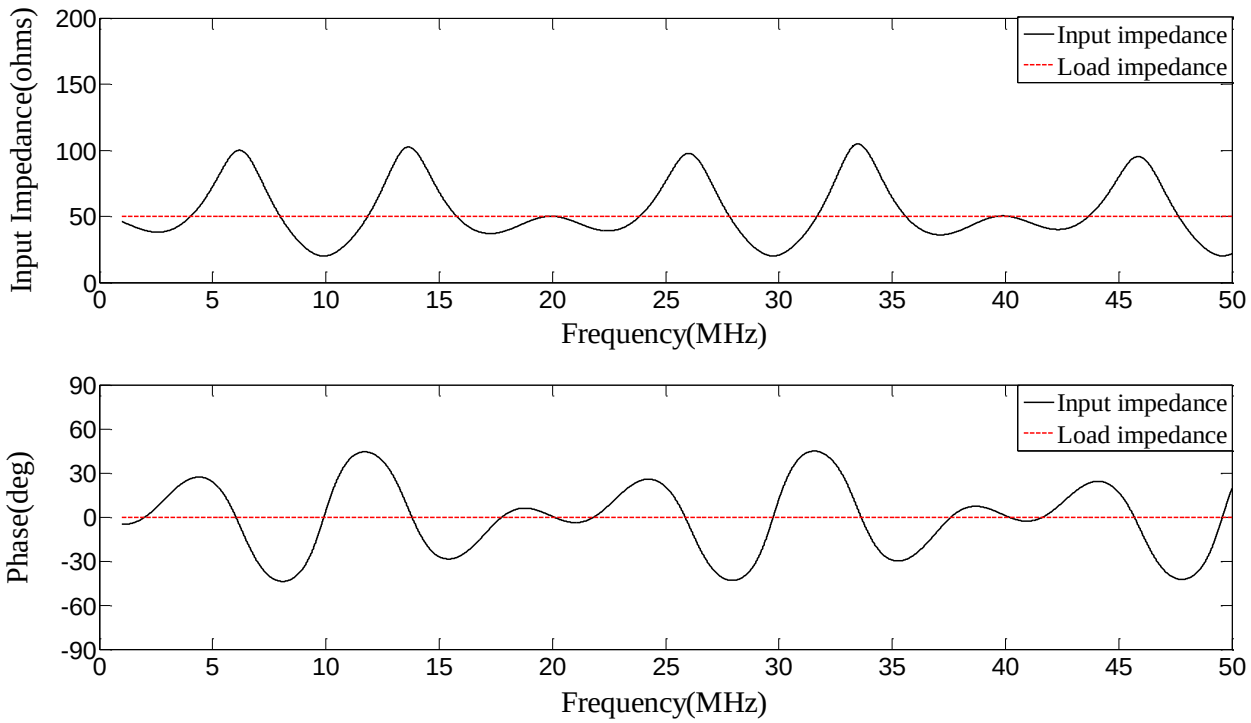

Figure 19. Variation in input impedance with frequency of wave transmission for SIMO topology (Z_{L1}=100 Ω and Z_{L2}=100 Ω and l=12.75 m, l_1=6.375 m

Figure 19 demonstrates another variation in input impedance for Z_{L1}= Z_{L2}= 100 Ω. The length of the TL network and TL-2 were chosen to be equal to 12.75 m and 6.375 m respectively. It is observed, that the input impedance satisfies (2.43) only at integral multiples of 20 MHz as the set of frequencies which satisfies $f = \frac{nv}{2l} = \frac{mv}{2l_2}$ is reduced. Reason being the TL-2 will now acts as quarter-wave transformer at 10 MHz and its odd integral multiples. The value of input impedance at these frequencies will now be given by Z_{in}=20 Ω.

It is noted that, the outlined approach is applicable for any other SIMO topology derived in Figure 16 and even if air instead of a conductive waveguide is the medium of transmission. For instance, if S_1 transfers power to L_2 and L_3 via the TL network followed, respectively, by TL-2

and TL-3, a set of frequencies of wave transmission is so determined such that (2.41) is satisfied using a newly-found Z_{in} in (2.42) that takes into account Z_{cl}, Z_{cl2} and $Z_{\mathrm{L}2}$, and Z_{cl3} and $Z_{\mathrm{L}3}$.

2.2.3. HFDPS with MIMO Topology

While several HFDPSs may emulate SISO and SIMO topologies, MIMO topologies, which involve simultaneous power transfer from plurality of sources to plurality of loads is often a reality. Consider a scenario illustrated in Figure 20, where source S_2 supplies power to L_2 of impedance $Z_{\mathrm{L}2}$ while source S_3 feeds power to L_3 of impedance $Z_{\mathrm{L}3}$. If each source feeds the respective load in a sequential manner, then, the signal integrity in such a scenario can be handled using the SISO methodology outlined under subsection 2.2.1, thereby determining a sets of frequencies, depending on the respective TL lengths ($l_2 = \frac{nv}{2f_2}$ and $l_3 = \frac{mv}{2f_3}$), which provide signal integrity by satisfying the conditions $Z_{in2} = Z_{\mathrm{L}2}$ and $Z_{in3} = Z_{\mathrm{L}3}$. Now, if only S_2 or S_3 feeds L_2 as well as L_3 at a time, then the network will emulate the SIMO topology and hence, a set of frequencies which ensure signal integrity can be determined following analysis under subsection 2.2.2. However, if both S_2 and S_3 as well as L_2 and L_3 are simultaneously active, such a MIMO scenario requires additional analysis that takes into account the effects of crosstalk in the TL network.

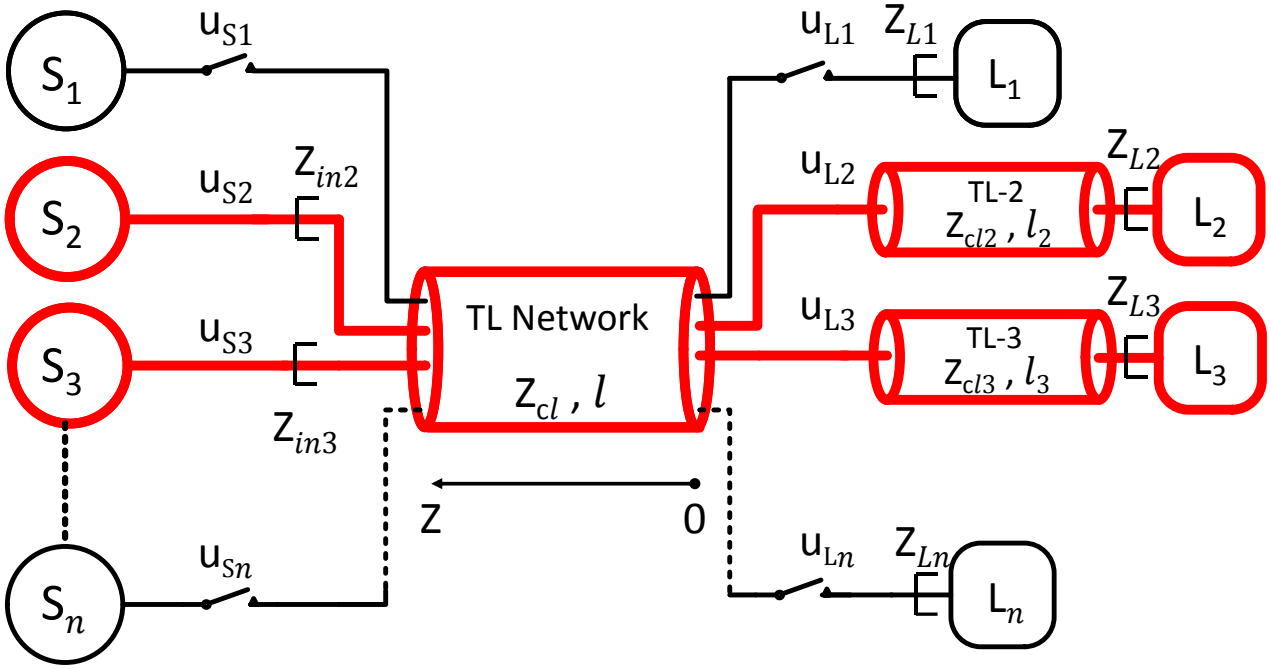

Figure 20. A MIMO topology showing simultaneous activation of plurality of sources and loads.

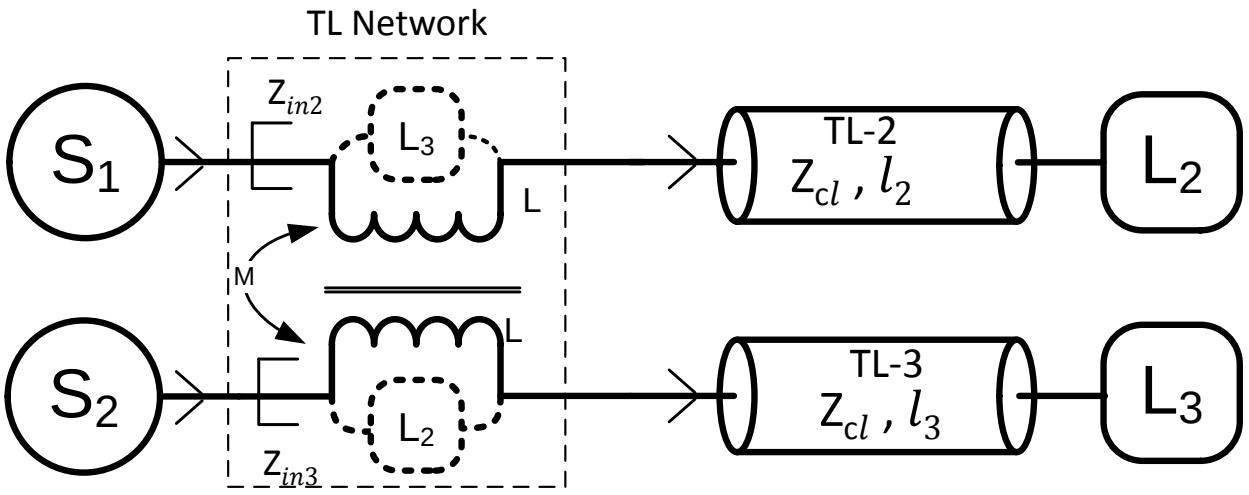

Figure 21. A simple embodiment of crosstalk in MIMO topology

A simple embodiment of such a crosstalk in a MIMO topology is illustrated in Figure 21, which shows a finite mutual coupling between the TL's that support power flow between S_2 and L_2 and S_3 and L_3.Due to this coupling, part of S_2's (S_3's) power is fed to L_3 (L_2) which is undesirable. In Figure 21, symbols M and L represent mutual inductance and self-inductances of the coupled inductor, respectively. Figure 22 and 23 illustrates the distribution of power supplied by source S_2 (S_3) with coefficient of coupling (K). It is observed that as coefficient of coupling or crosstalk between two individual SISO topologies increases, part of the power as shown in blue in Figure 22 and 23 is transferred to load L_3 and L_2 respectively. It can be realized as if load L_3 (L_2) is referred at the input of S_2 (S_3) in parallel with mutual inductance as shown in Figure 21.

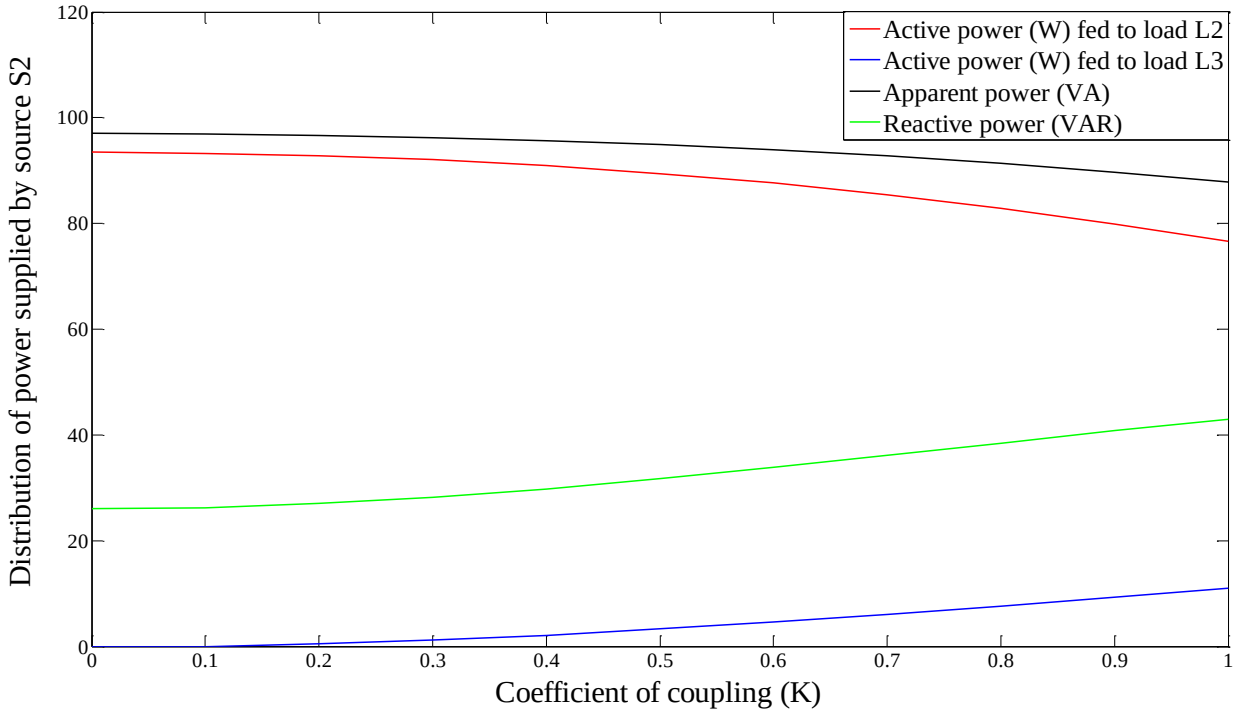

Figure 22. Variation in distribution of power supplied by source S_2 (when S_3 and L_3 are active) with coefficient of coupling (K).

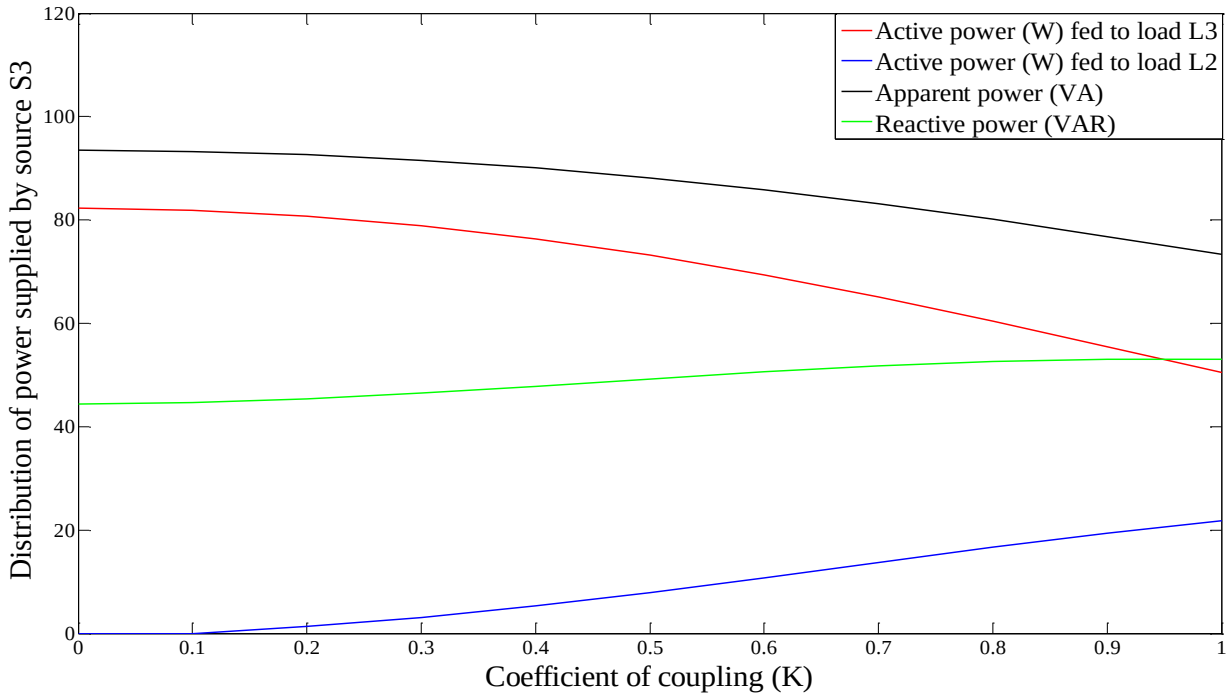

Figure 23. Variation in distribution of power supplied by source S_3 (when S_2 and L_2 are active) with coefficient of coupling (K).

Hence the input impedances seen by S_2 (row 1) and S_3 (row 2) are given by following:

$$\begin{bmatrix} Z_{in2} \\ Z_{in3} \end{bmatrix} = \begin{bmatrix} Z_{22} \parallel Z_{23} \\ Z_{32} \parallel Z_{33} \end{bmatrix} \tag{2.44}$$

where Z_{22} (Z_{33}) is the impedance seen by S_2 (S_3) when S_3(S_2) and L_3 (L_2) are inactive and Z_{23} (Z_{32}) is the impedance seen by S_2 (S_3) when S_3(S_2) and L_2 (L_3) are active. To ensure signal integrity, the following conditions need to be satisfied:

$$Z_{22} = Z_{L2} \text{ and } Z_{33} = Z_{L3} \tag{2.45}$$

$$Z_{23} = Z_{32} = \infty. \tag{2.46}$$

Condition (2.45) ensures signal integrity in the absence of crosstalk while (2.46) is the condition for eliminating crosstalk. One way to practically satisfy (2.46) is to ensure negligible mutual inductance (or mutual coupling) for the system shown in Figure 21. Because this solution is not generic, an alternative approach, as shown in Figure 24, is to use a band-stop filter in the power transmission path between S_2 (S_3) to L_2 (L_3).

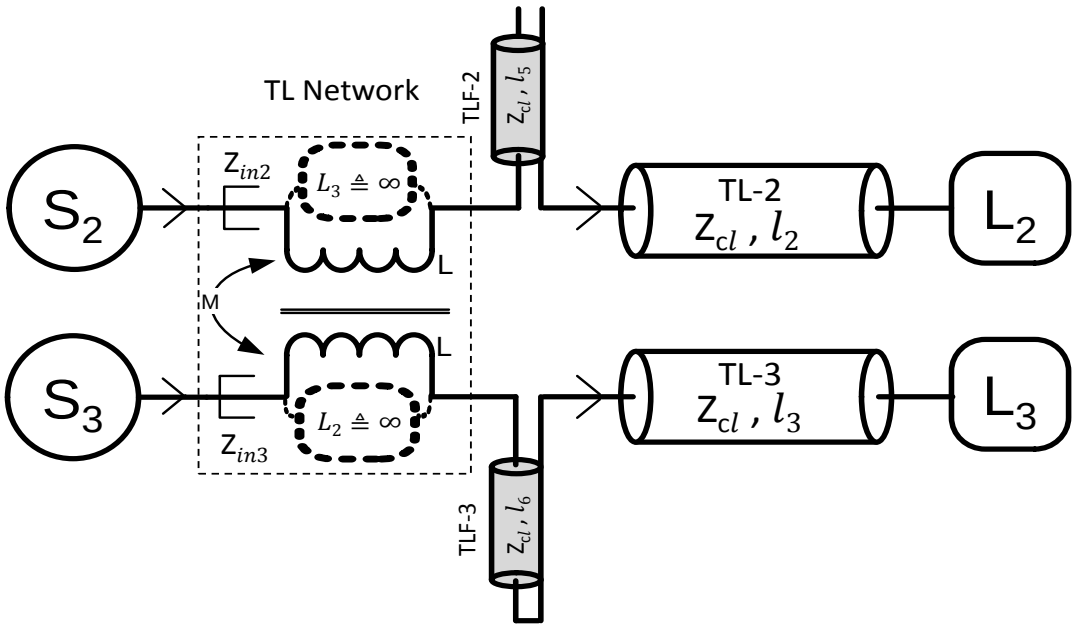

Figure 24. Mitigation of crosstalk in Figure 21 using tuned TL-based band-stop filters

This Dissertation uses a TL-based band-stop filter [26], as outlined in Appendix A, to exploit the periodic property of such a filter. The basic idea (following SISO topology in subsection 2.2.1) is to initially select a set of frequency of wave transmission between S_2 (S_3) and L_2 (L_3) such that the condition for signal integrity following (2.45) is achieved assuming no crosstalk. Subsequently, the band-stop filter for each of these paths is placed and so tuned such that it only lets go the power signal at the selected frequency of wave transmission. Thus, for the MIMO topology, any cross talk between S_2 (S_3) and L_3 (L_2) is essentially eliminated and power flows from S_2 (S_3) and L_2 (L_3) without signal-integrity issues. Figures 25 and 26 represent the distribution of power supplied

by source S2 (S3) with coefficient of coupling using TLF-2 (TLF-3) as a band-stop filters as shown in Figure 24.

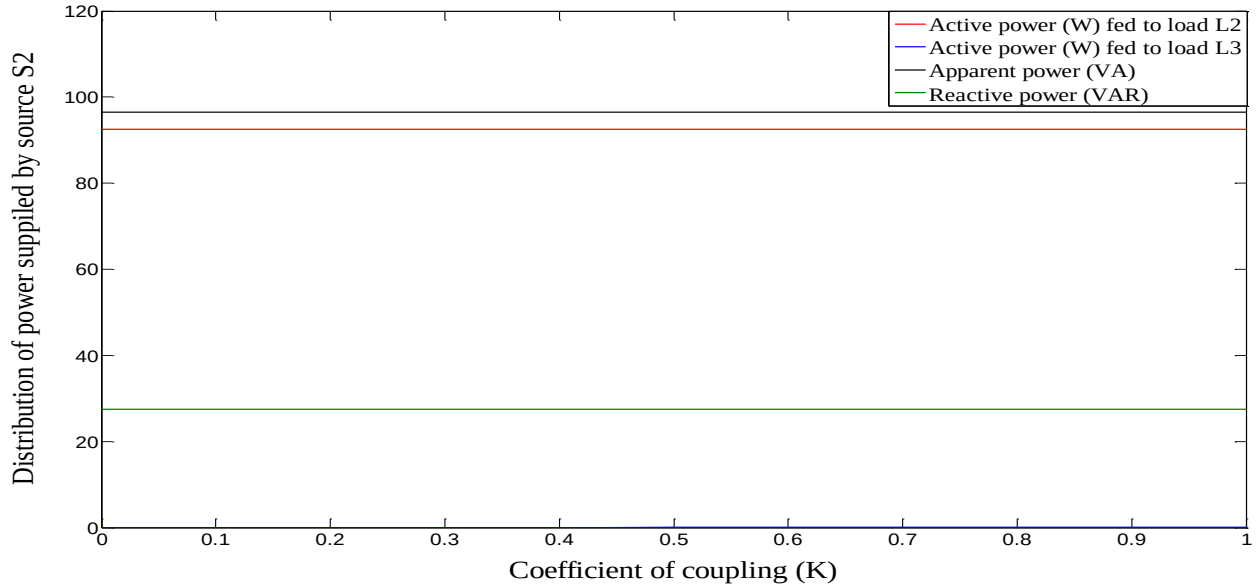

Figure 25. Variation in distribution of power supplied by source S_2 (when S_3 and L_3 are active) with coefficient of coupling (K) using TLF-2 and TLF-3.

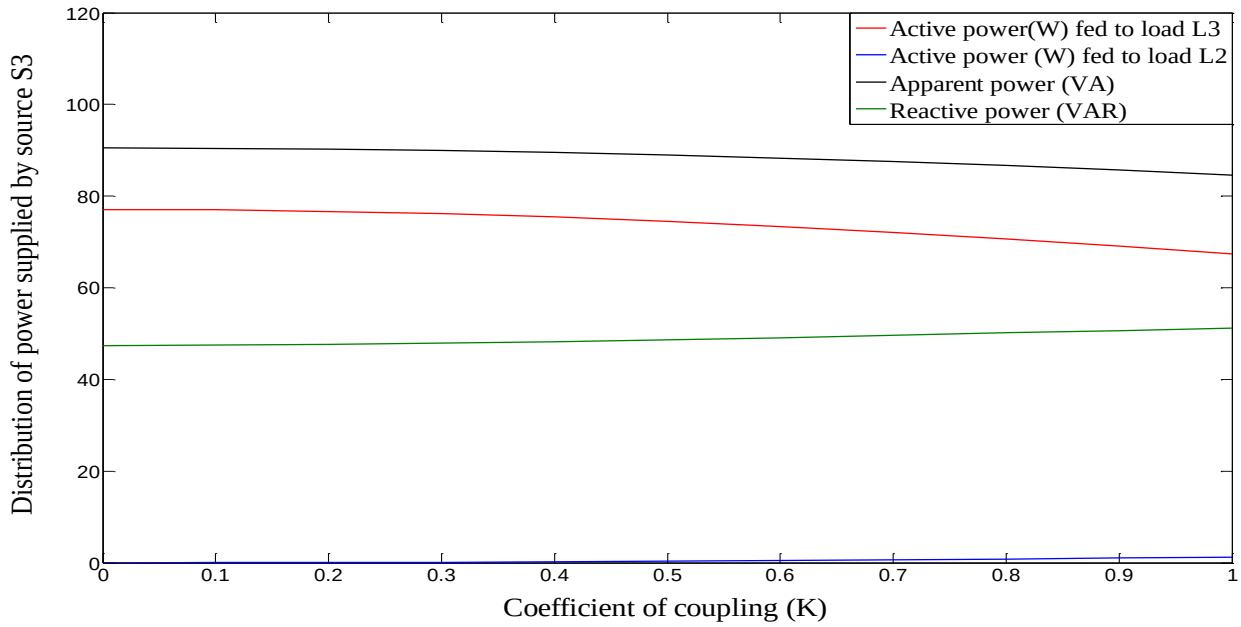

Figure 26. Variation in distribution of power supplied by source S_3 (when S_2 and L_2 are active) with coefficient of coupling (K) using TLF-2 and TLF-3.

It is observed that, the power fed by S_2 (S_3) to load L_3 (L_2) can be minimized by employing the TL based band-stop filters.

CHAPTER III. RESULTS

3.1. Experimental Setup

In this chapter, for the proof of concept, an experimental setup as shown in Figure 27 was developed for the validation of frequency-dependent criterion as outlined in chapter II and extended for SISO, SIMO and MIMO topologies. Table 3 illustrates the instruments used for frequency domain as well as time domain validation and testing. Also, this chapter includes the simulated prametric analyses for SISO and SIMO and experimental parametric analyses for MIMO topology.

Table 3. Instrumentation required for the validation of frequency and time-domain analyses.

Model No.	Make	Function
HP 3577A	Hewlett-Packard	Vector network analyzer (VNA) for measurment of the network parameters of electrical networks (S parameters, Smith chart, frequency response.
HP 35677A	Hewlett-Packard	
ENI 503 L	Bell Electronics	RF power amplifier capable of amplifying any laboratory signal or sweep generator
7977A	Belden	Transmission line coaxial cable with parameters tabulated in table 1.
AFG3252	Tektronix	Signal generator
CHF1105DCBF	Bourns	Resistive loads

VNA was used together with S-parameter test set to carry out the frequency domain testing of the TL network. S-parameters, also known as scattering parameters refers to a discontinuity or obstruction encounterd by electromagnetic waves due to dissimilar dielectric media. To measure the gravity of such discontinuity, a TL network can be modelled as two port network as shown in Figure 28. Z_L , Z_S and Z_{cl} represents the load impedance, source impedance and chartersitic impedance respectively. Four S-parameters S_{11}, S_{22}, S_{12}, S_{21} are used to determine the impedance offered by the discontinuity and its effects on incident voltage and current signals. S_{11}, S_{22} measures the reflection coefficient of voltage at the input port and output port of the transmission line network respectively whereas S_{12}, S_{21} represents the transmission coefficient or reverse and forwrad voltage gain respectively .

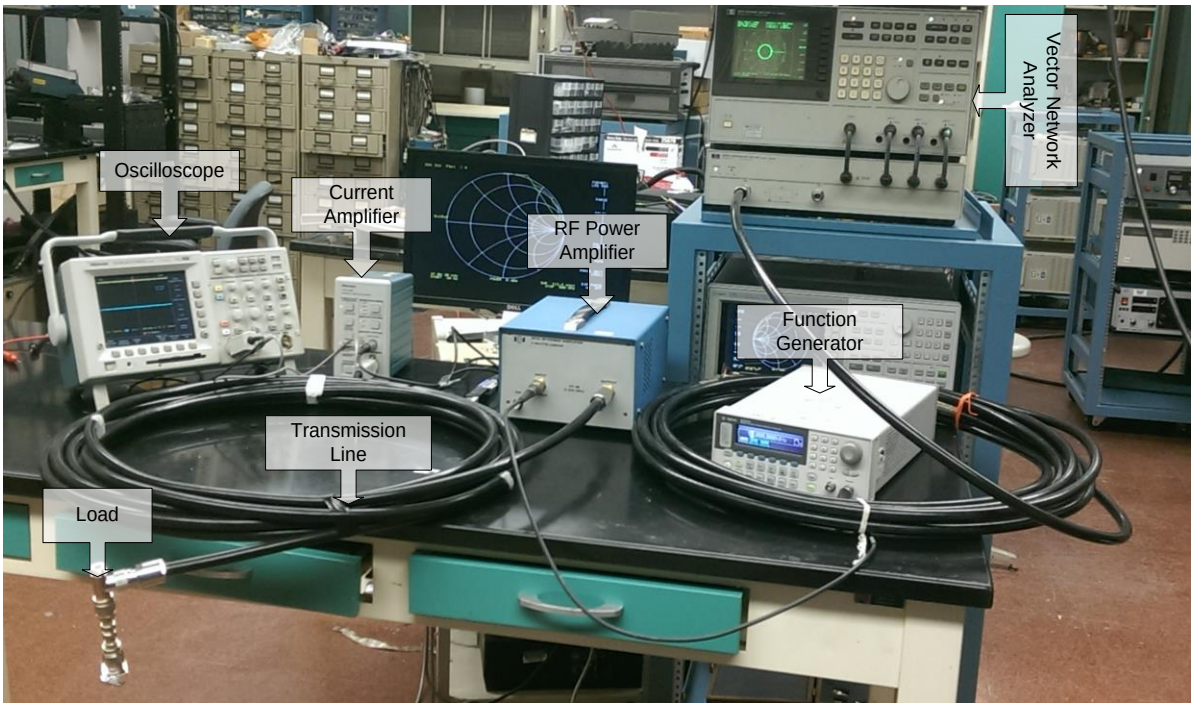

Figure 27. Experimental setup for validation of frequency selection criterion.

For our experimental validation, S_{11} parameter will be used as a reference to measure the reflection coefficient at the input of the transmission line network. Since, VNA does not measure

the input impedance, instead S_{11} parameter will be used to calculate its value by following expression

$$Z_{in} = Z_{cl}\frac{S_{11}+1}{1-S_{11}} \quad (4.1)$$

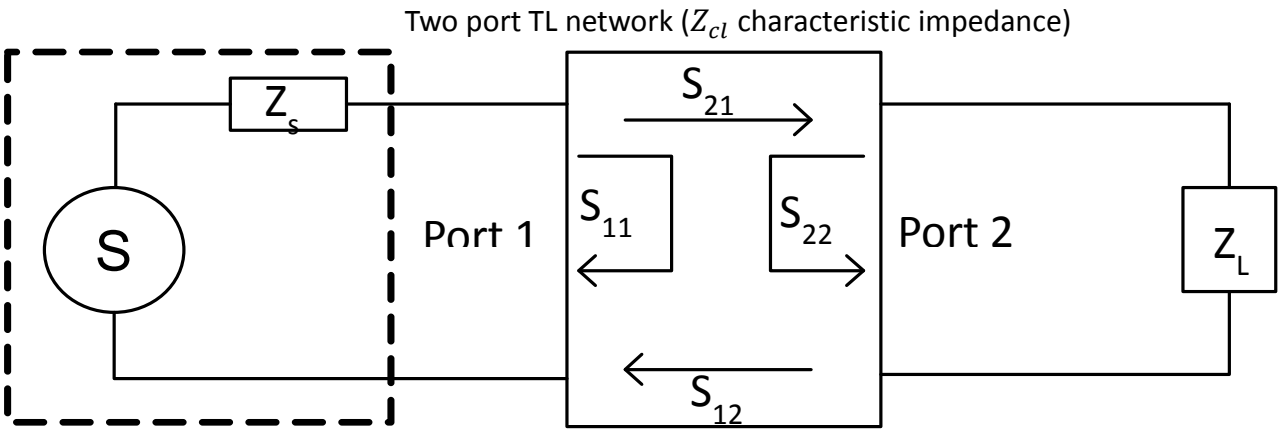

Figure 28. A representation of scattering parameters in two port TL network.

The time- domain analyses have been carried out at an operating frequency of 10 MHz in order to limit the size of the experimental setup.

3.2. HFDPS with SISO topology

Figure 29 demonstrates the magnitude and phase variation of normalized input impedance (with respect to characteristic impedance of the transmission line) with frequency of wave transmission using a Smith chart for the SISO topology as shown in Figure 7. A Smith chart is a graphical tool to represent the behavior of high frequency circuits. It represents all possible complex impedances in form of reflection coefficient. In Figure 29, the horizontal line divides the Smith chart in two planes. Top-half plane represents inductive behavior of the electrical network whereas bottom-half represents capacitve behavior of the network. The horizontal line in the chart

is the representation of resistive behavior of the network. The numbers and their location marked on the chart represents the magnitude and phase of the normalized input impedance. To test the frequency domain aspect of the SISO topology, a transmission line length of 12.75 m and load of impedance Z_{L1}= 100 Ω were used. It can be seen from the Smith chart that, the normalized input impedance (Z_{in}/Z_{cl}) curve intersects the horizontal line at 0.5 and 2, which corresponds to 25 Ω and 100 Ω respectively. Also, the chart illustates that, the input impedacne exhibits inductive beahvior in top half plane and capacitive behavior in bottom half plane owing to the transmission-line effects. It should be noted, that the input impedacne is resistive in nature at 0.5 corresponding to the frequency set obtained using (2.39b) which lies at integral multiples of 5 MHz thereby satisfying (2.38b) or $Z_{in} = {Z_{cl}}^2/Z_{L1} = 25$ Ω. But, (2.38a) or $Z_{in} = Z_L = 100$ Ω is satisfied only at frequencies set obtained using (2.39c) which lies at integral multiples of 10 MHz.

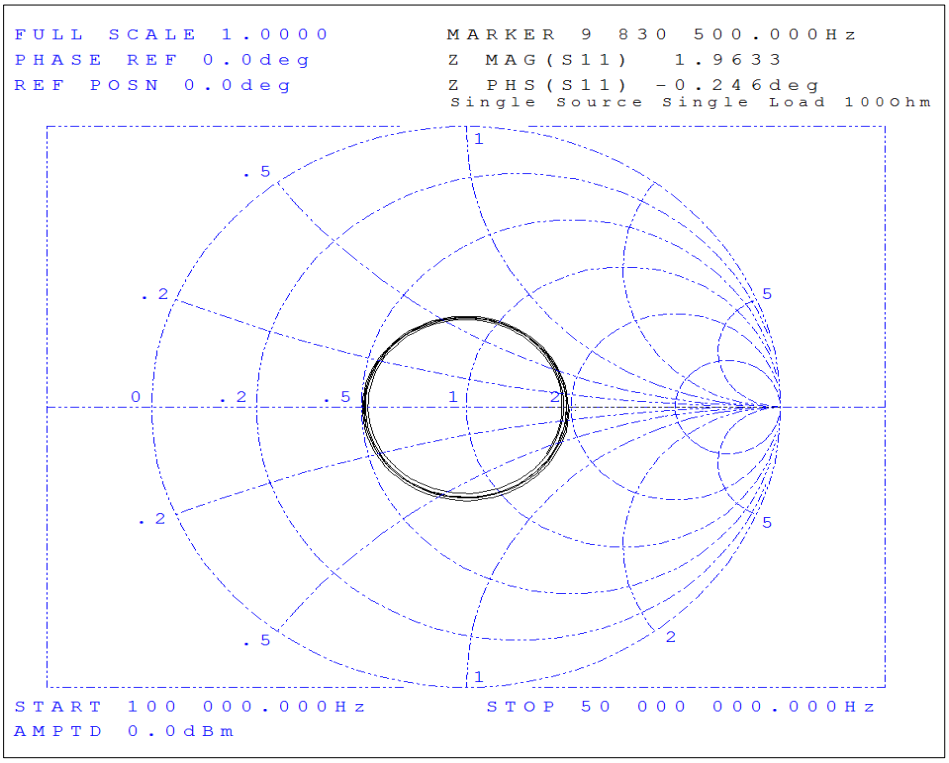

Figure 29. Variation in normalized input impedance with frequency of wave transmission for SISO topology using Smith chart

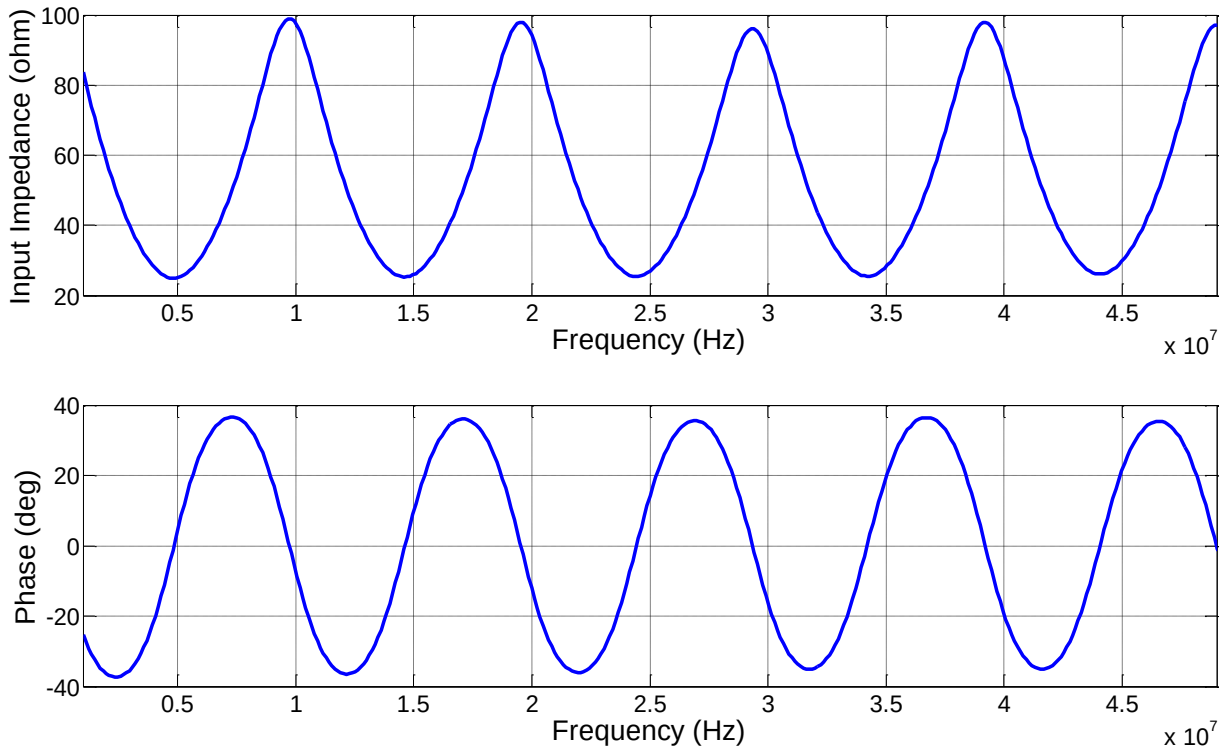

Figure 30. Magnitude and phase variation of input impedance with frequency of wave transmission

The magnitude and phase variation of the input impedance for the SISO toppology as shown in Figure 7 is illustrated by Figure 30. The data points for Figure 30 were extracted following (4.1) from S_{11} parameter obtained using VNA. Figure 30 displays that, at integral multiples of 5 MHz and 10 MHz the input impedance is resistive in nature (zero phase angle) and its value is given by 25 Ω and 100 Ω respectively. It can also be observed, that the variation is periodic in nature, and closely follows the simulation result in Figure 9 for a TL network length of 12.75 m.

Figure 31 displays the time domain results for the same SISO topology. Voltage and current were measured at the input of transmission line network. Figures 31 (a) and 31(d) shows that, the current and voltage are in phase with each other. Also, input impedance (Z_{in}) closely matches load impedance only at 10 MHz and 20 MHz which are a subset of the set of frequencies obtained from (2.39c) for a particular length of the transmission line network, follows from frequency domain

results. Figure 31(b) illustrates that, when frequency of wave transmission does not follow (2.39c), the input impedance exhibits capacitve behavior with magnitude and phase of 60.43 Ω and -34.128 degree respectively and can also be calculated from (2.37). However, at 15 MHz in Figure 31(c), the input impedance is resistive in nature and its value is given by 25 Ω, which corresponds to 0.5 (normalize input impedance) in Smith chart in Figure 29. For this frequency the transmission line behaves as a quarter wave transformer of length equivalent to $3\lambda/4$, which follows from (2.39b).

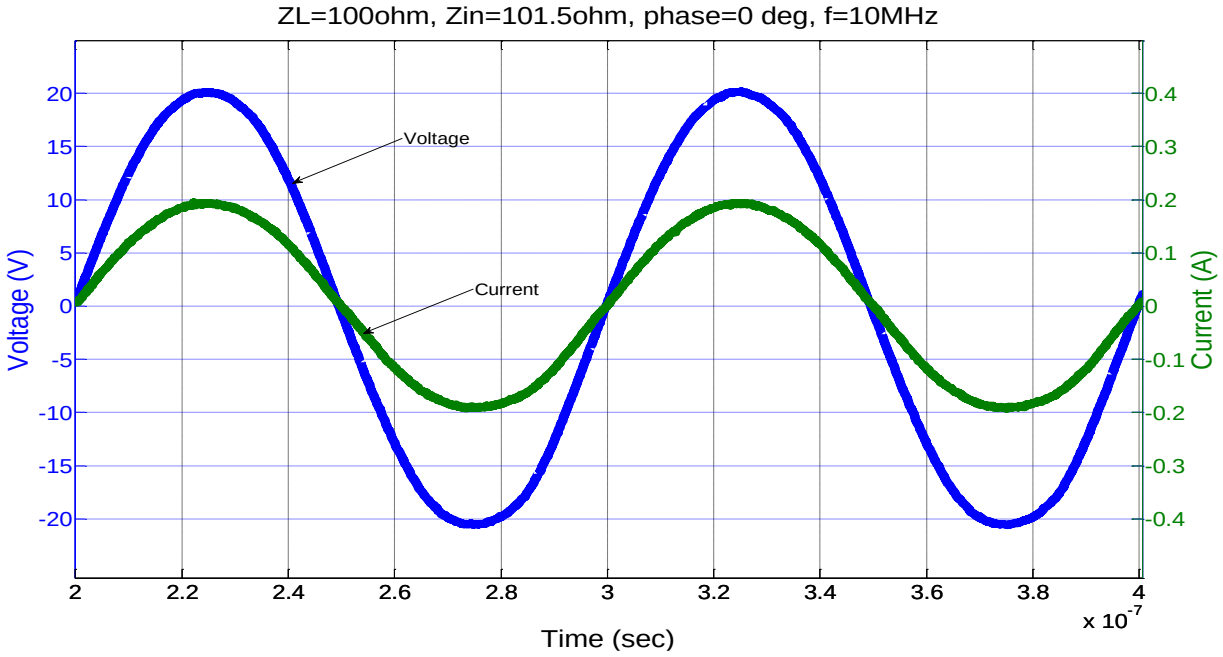

(a)

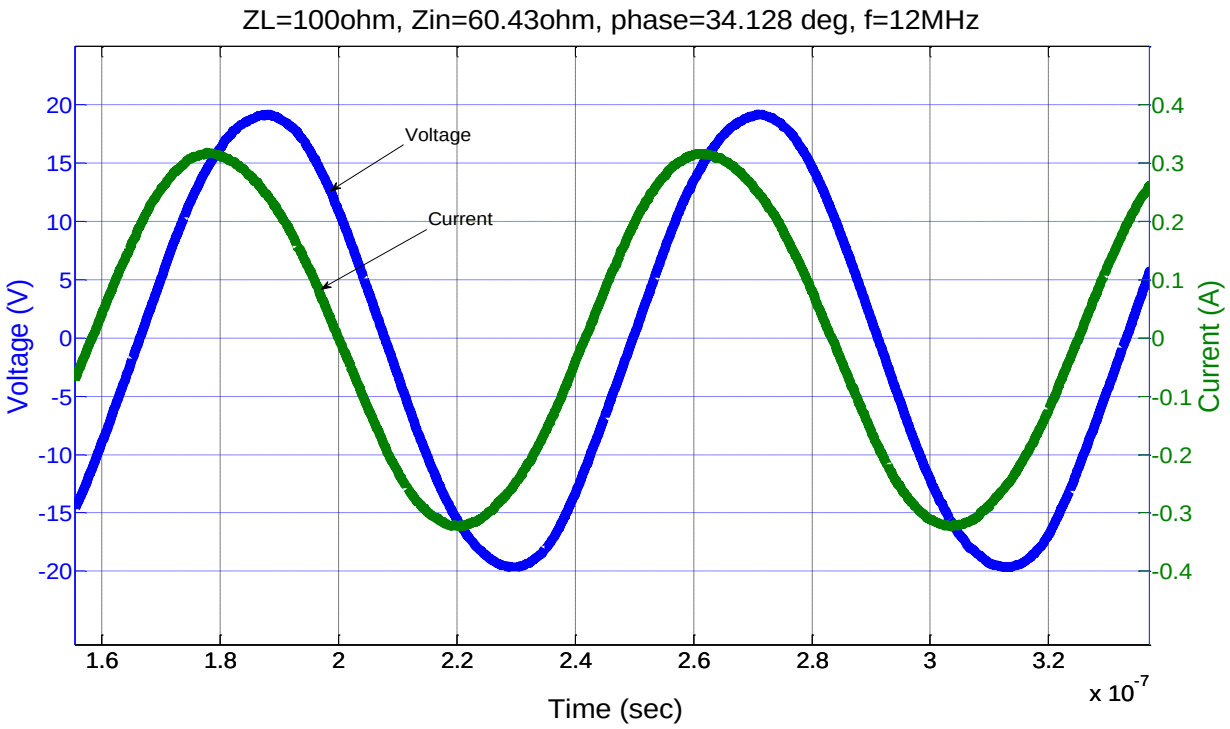
ZL=100ohm, Zin=60.43ohm, phase=34.128 deg, f=12MHz
Voltage
Current
Voltage (V)
Current (A)
Time (sec)
x 10^-7
20
15
10
5
0
-5
-10
-15
-20
0.4
0.3
0.2
0.1
0
-0.1
-0.2
-0.3
-0.4
1.6
1.8
2
2.2
2.4
2.6
2.8
3
3.2

(b)

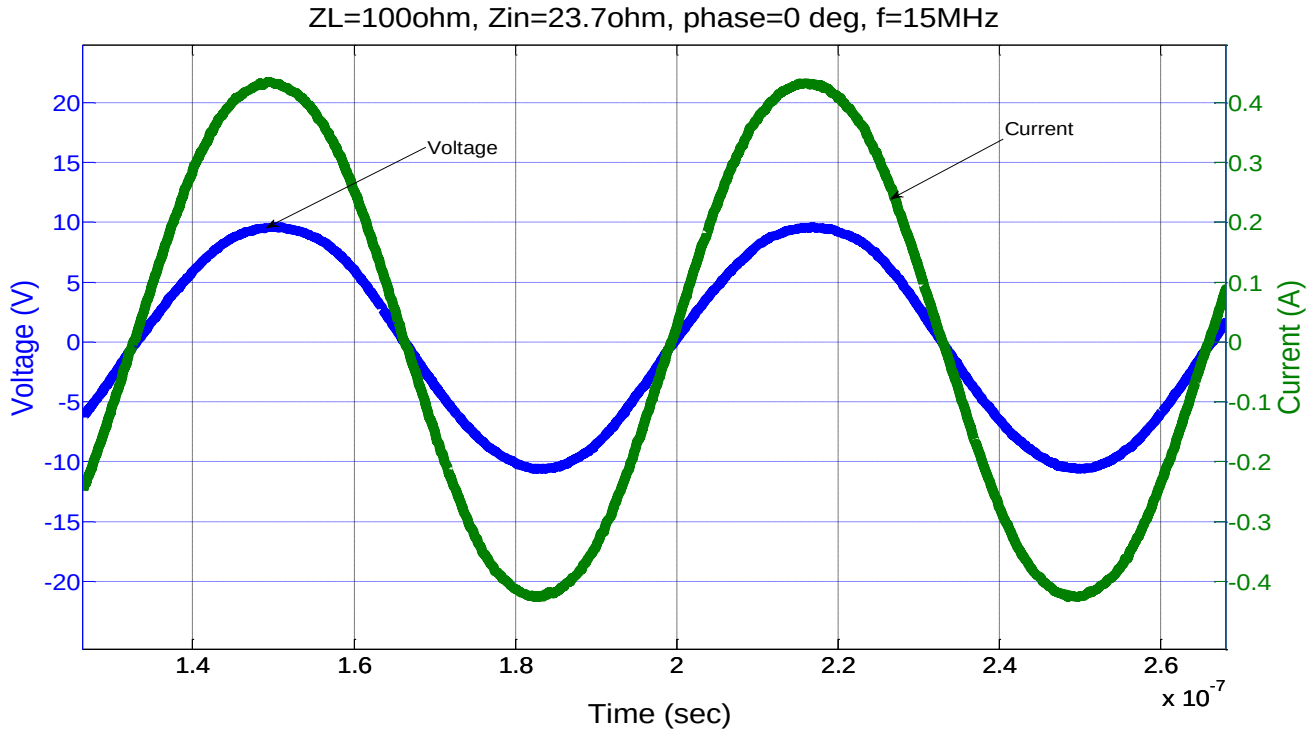
ZL=100ohm, Zin=23.7ohm, phase=0 deg, f=15MHz
Voltage
Current
Voltage (V)
Current (A)
Time (sec)
x 10^-7
20
15
10
5
0
-5
-10
-15
-20
0.4
0.3
0.2
0.1
0
-0.1
-0.2
-0.3
-0.4
1.4
1.6
1.8
2
2.2
2.4
2.6

(c)

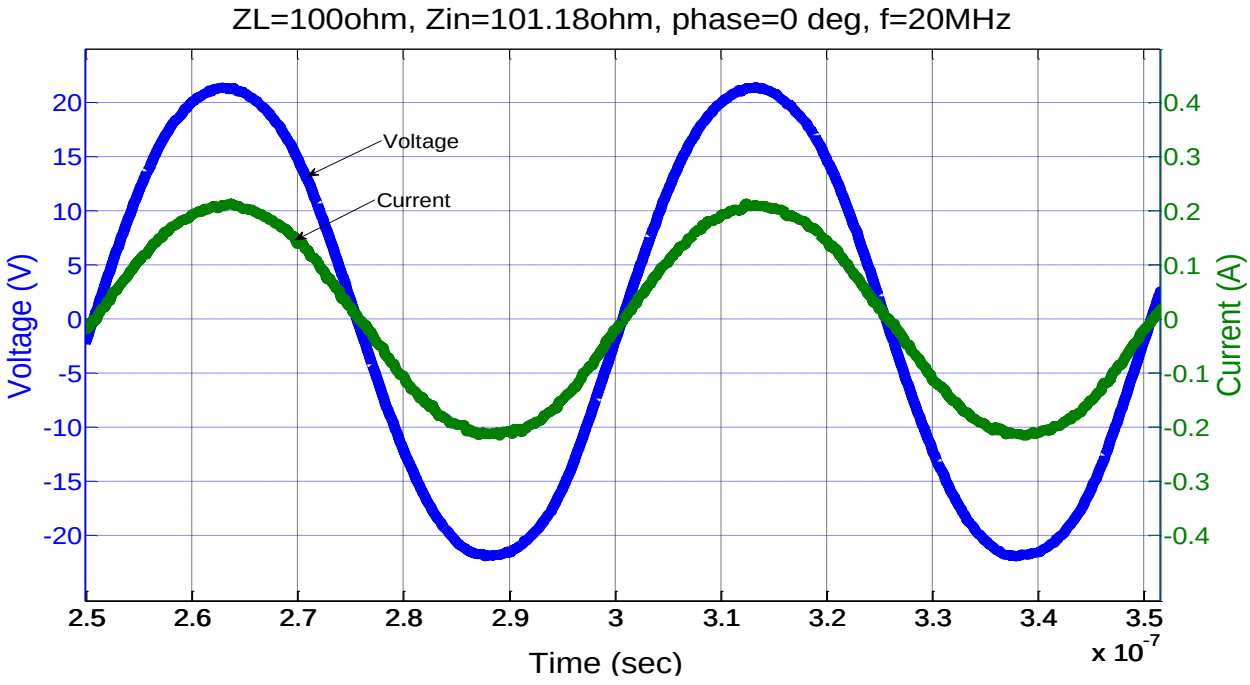

(d)

Figure 31. Input voltage and input current for SISO topology at frequency of wave transmission (a) 10 MHz (b) 12 MHz (c) 15 MHz (d) 20 MHz

Figure 32 represents a simulated 3-D parametric variation of input impedance (marked with Z) with frequency of wave transmission (marked with X) and length of the TL (marked with Y). It can be seen that the input impedance calculated with time domain plots are captured by the four points marked by A1, A2, A3 and A4 on the curve in Figure 32.

Figure 33 represents another simulated 3-D parametric variation of input impedance (marked with Z) with variation in TL parameters i.e. velocity of propagation in the TL network (marked with Y) and length of the TL network (marked with X). The points B1, B2, B3 and B4 on the curve signifies that, keeping the frequency of wave transmission constant, (2.38a) can still be satisfied for different length of the TL and different TL properties. The red area in Figures 32 and 33 represents the points at which (2.38a) is satisfied.

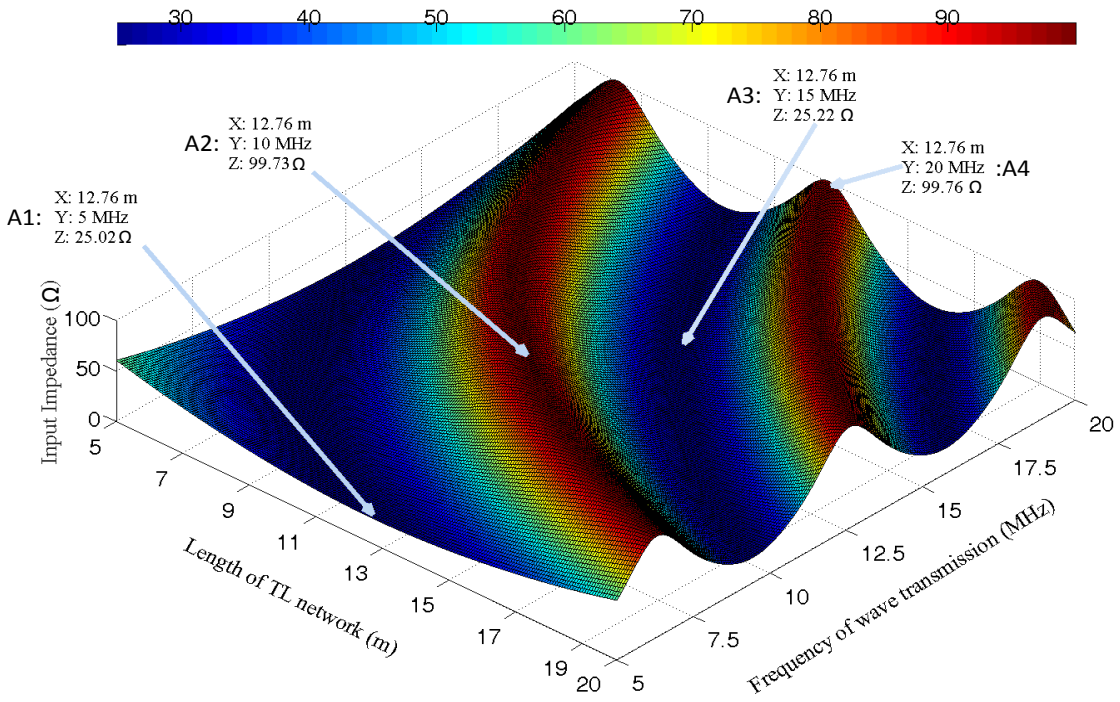

Figure 32.Variation in input impedance (marked with Z) with frequency of wave transmission (marked by Y) and TL network length (marked by X) for a SISO topology.

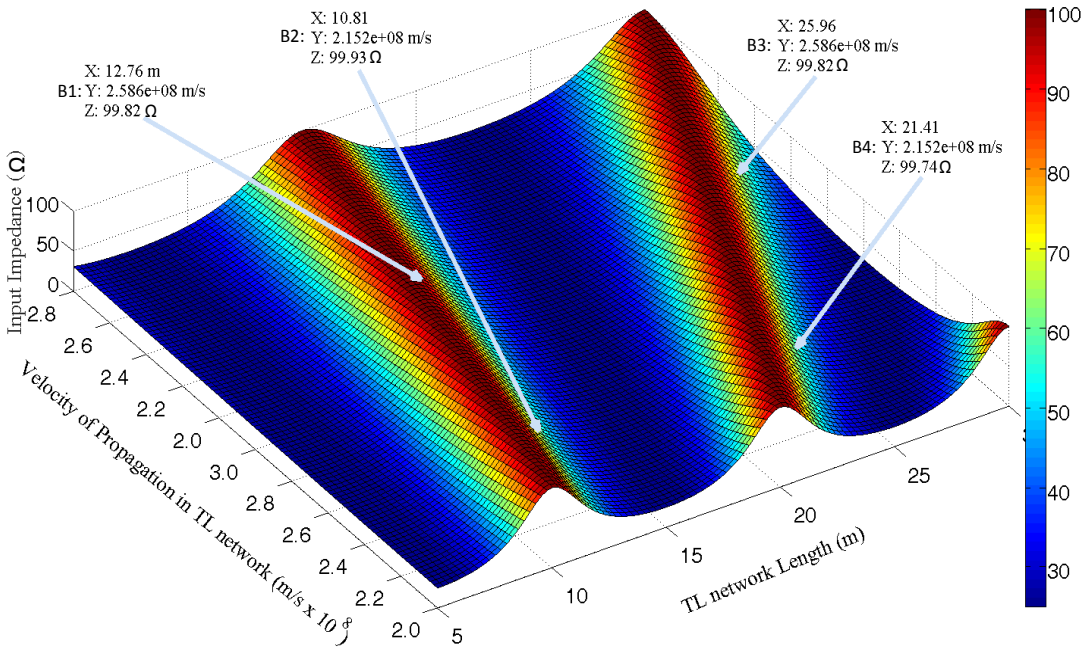

Figure 33. Variation in input impedance (marked by Z) with variation in velocity of propagation (marked by Y) and TL network length (marked by X) at a wave transmission frequency of 10 MHz for a SISO topology.

3.3. HFDPS with SIMO topology

For SIMO topology frequency domain validation, both, the length of TL network (l) and TL-2 (l_2) were chosen to be equal to 12.75 m. Two loads of impedance Z_{L1}= 100 Ω and Z_{L2}= 100 Ω were selected. Figure 34 illustrates the frequency domain plot for SIMO topology as shown in Figure 16, in form of Smith chart. It can be seen that, the normalized input impedance varies between 0.64-2.4 p.u. which corresponds to range of 32 Ω to 122 Ω respectively. Also, the normalized input impedance exhibits capacitive behavior at its minimum value and resistive nature at its maximum value. Figure 35 represents the variation of input impedance with frequency of wave transmission. It can be observed that, at integral multiples of 10 MHz which satisfy $f = \frac{nv}{2l}$ = $\frac{mv}{2l_2}$, input impedance is given by parallel combination of Z_{L1} and Z_{L2} and aproaches 50 which can also be confirmed from Smith chart when the value of normalized input impedance approaches 1.

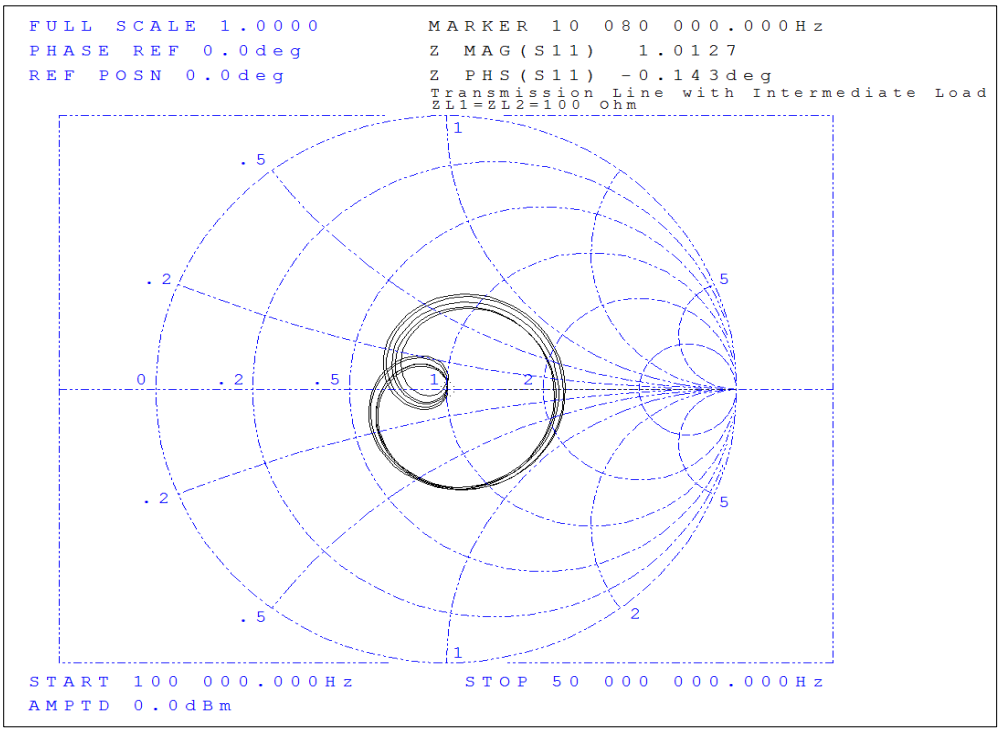

Figure 34. Variation in normalized input impedance with frequency of wave transmission for SIMO topology using Smith chart

However at odd integral multiples of 5 MHz, TL network and TL-2 act as a quarter wave transformer and the input impedance approaches 22 Ω. Figure 36 displays the time variation aspect of input voltage and input current for SIMO topology as shown in Figure 16. The measurements were taken at the input port of the TL network. Figure 36 (a) and 36 (d) shows that voltage and current are in phase with each other at frequency of 10 MHz and 20 MHz respectively. As these frequencies do satisfy $f = \frac{nv}{2l} = \frac{mv}{2l_2}$, the input impedance approaches 52.3 Ω, which closely matches frequency domain results in Figure 17. Also at 15 MHz, as evident from Figure 36 (c), voltage and current are in phase with each other, but input impedance approaches 122 Ω due to the behavior of TL network and TL-2 as a quarter wave transformer. At 13 MHz, which does not lie in the frequency subset that satisfies (2.43), displays inductive behavior with magnitude and phase angle of 41.52 Ω and 30.5 degree respectively owing to the transmission-line effects.

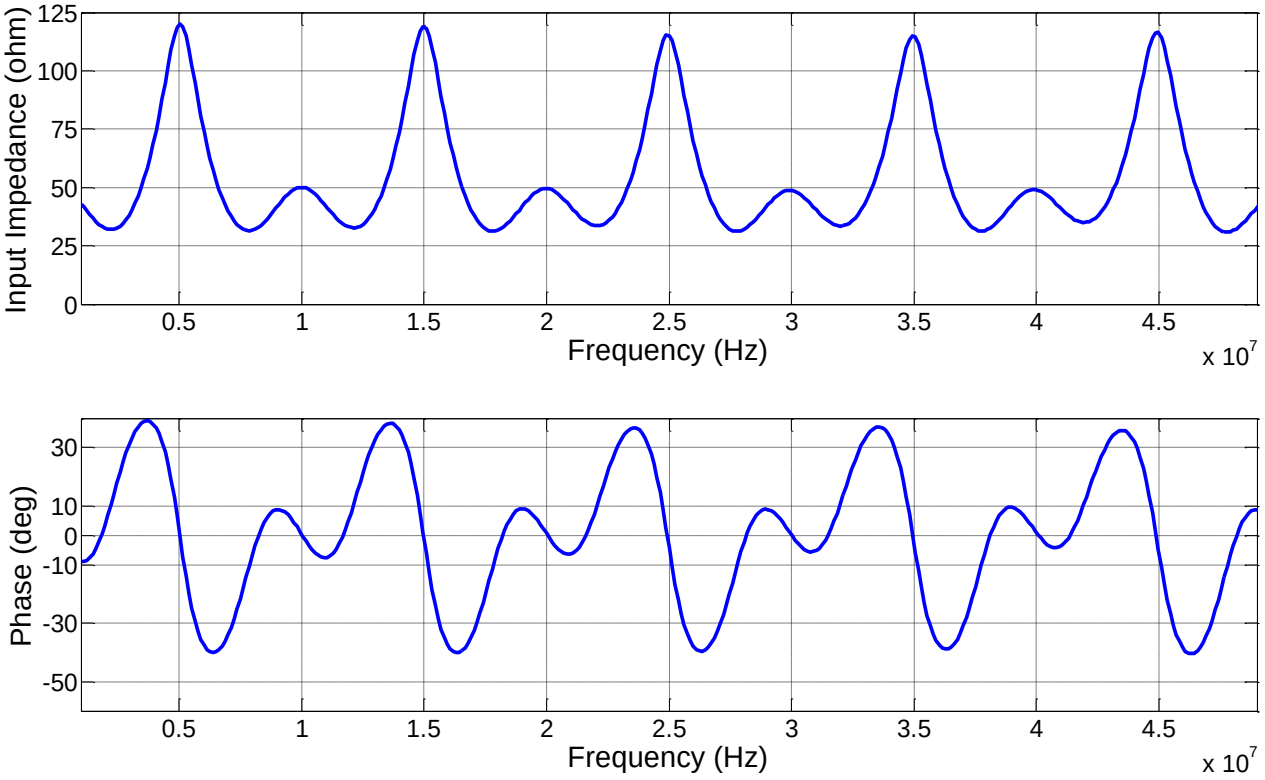

Figure 35. Variation of input impedance with frequency of wave transmission for SIMO topology

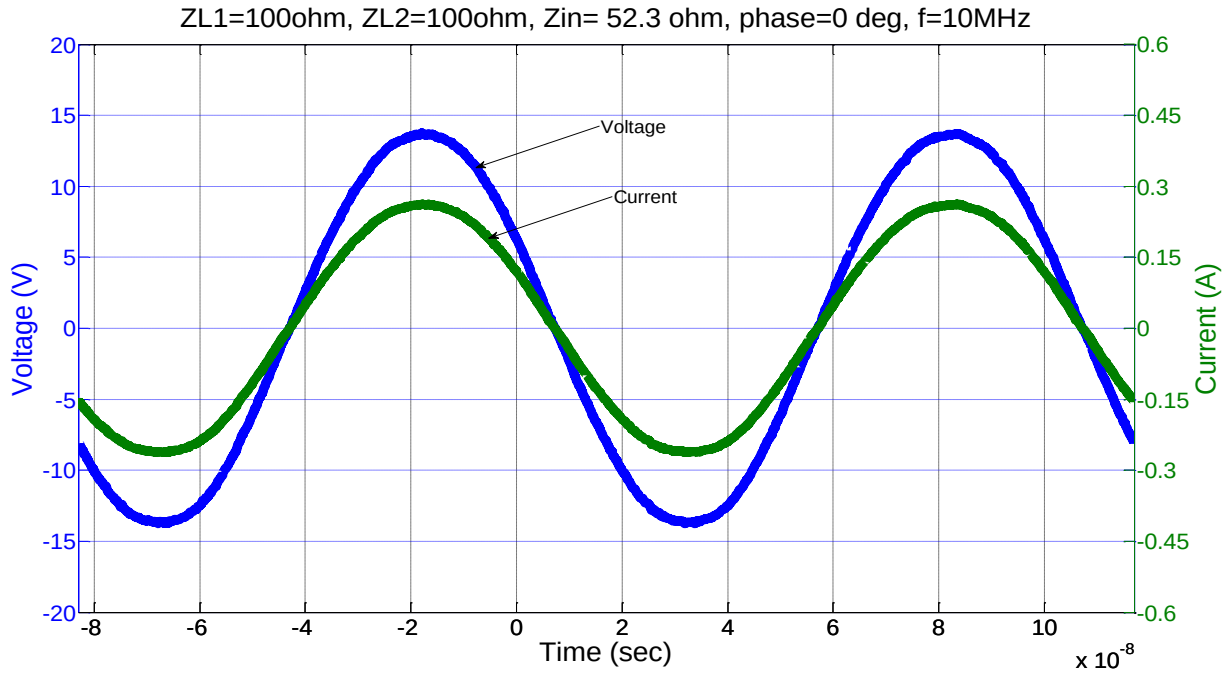

(a)

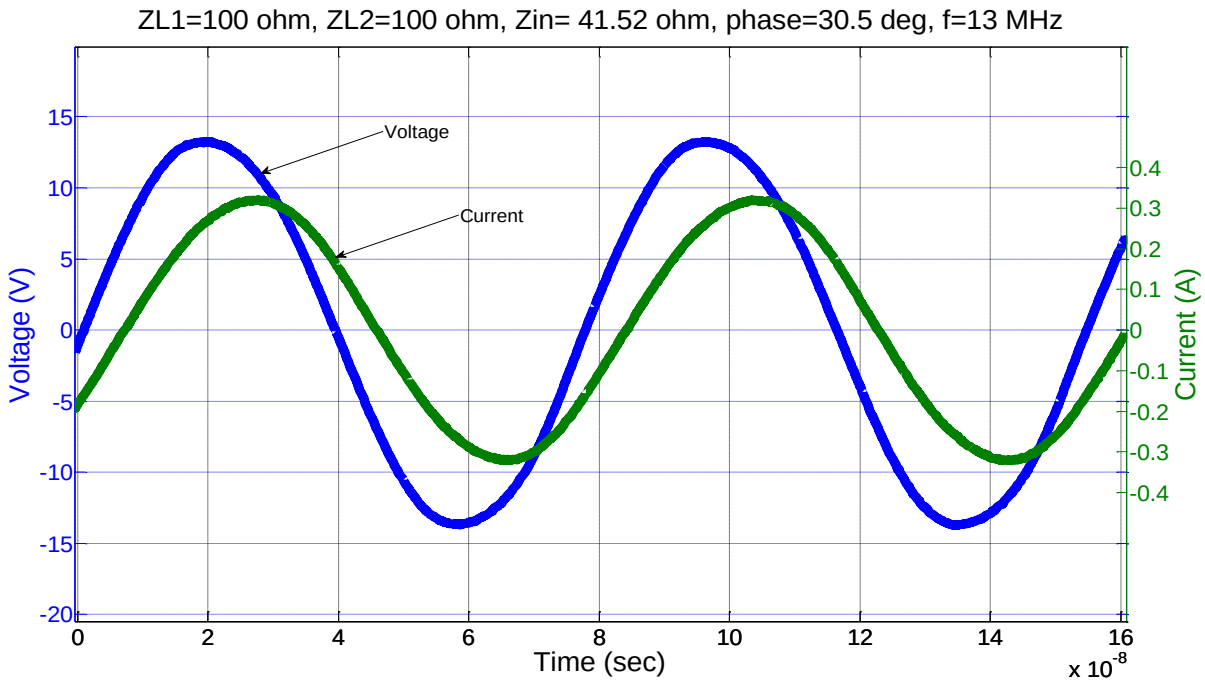
ZL1=100 ohm, ZL2=100 ohm, Zin= 41.52 ohm, phase=30.5 deg, f=13 MHz
Voltage
Current
Voltage (V)
Current (A)
Time (sec)
x 10^-8

(b)

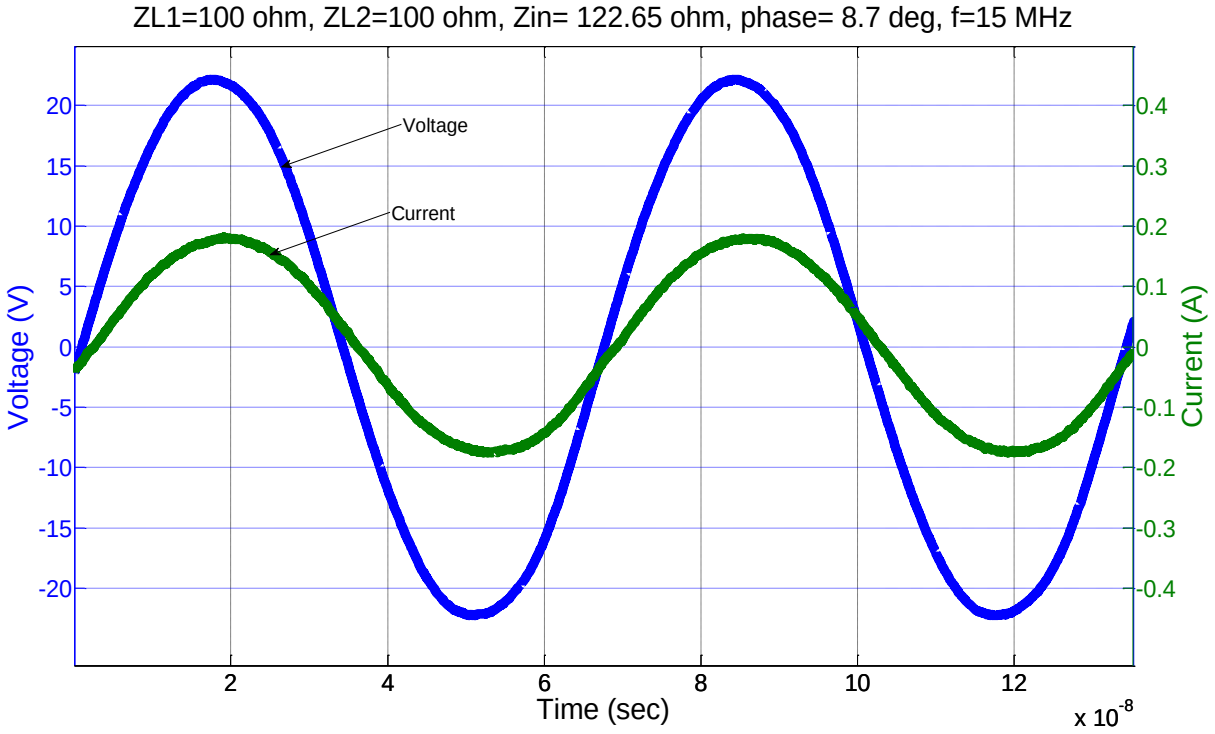
ZL1=100 ohm, ZL2=100 ohm, Zin= 122.65 ohm, phase= 8.7 deg, f=15 MHz
Voltage
Current
Voltage (V)
Current (A)
Time (sec)
x 10^-8

(c)

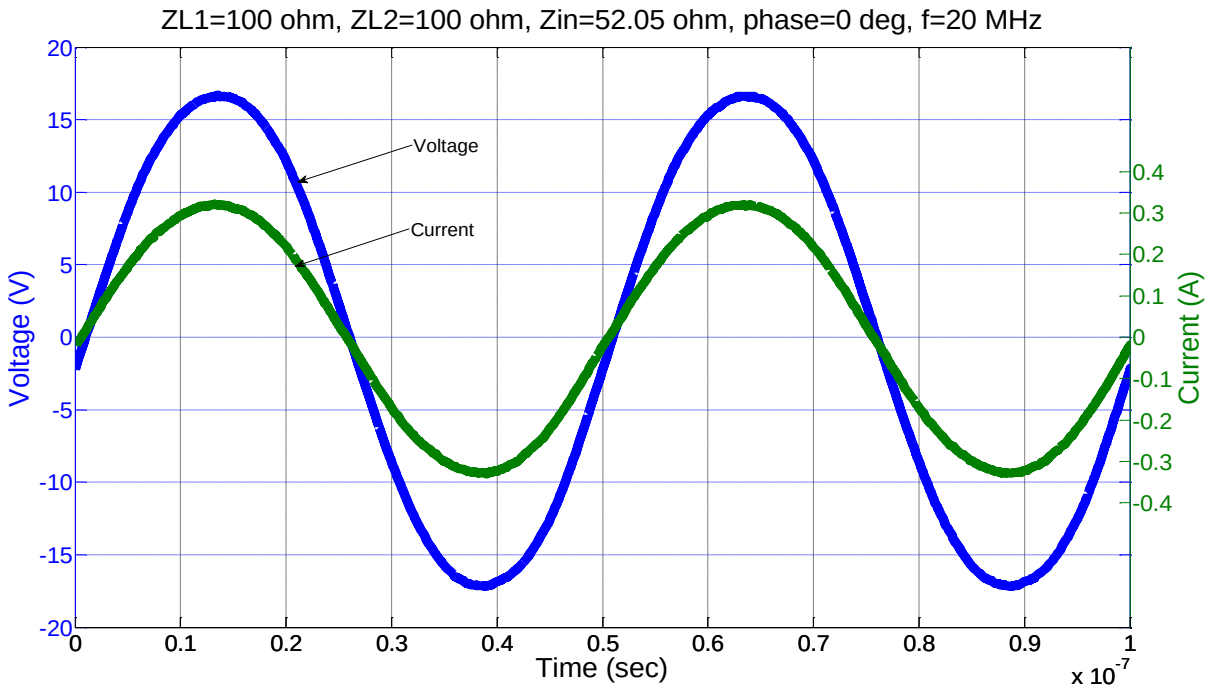

(d)

Figure 36. Input voltage and input current for SIMO topology at frequency of wave transmission (a) 10MHz (b) 13 MHz (c) 15 MHz (d) 20MHz

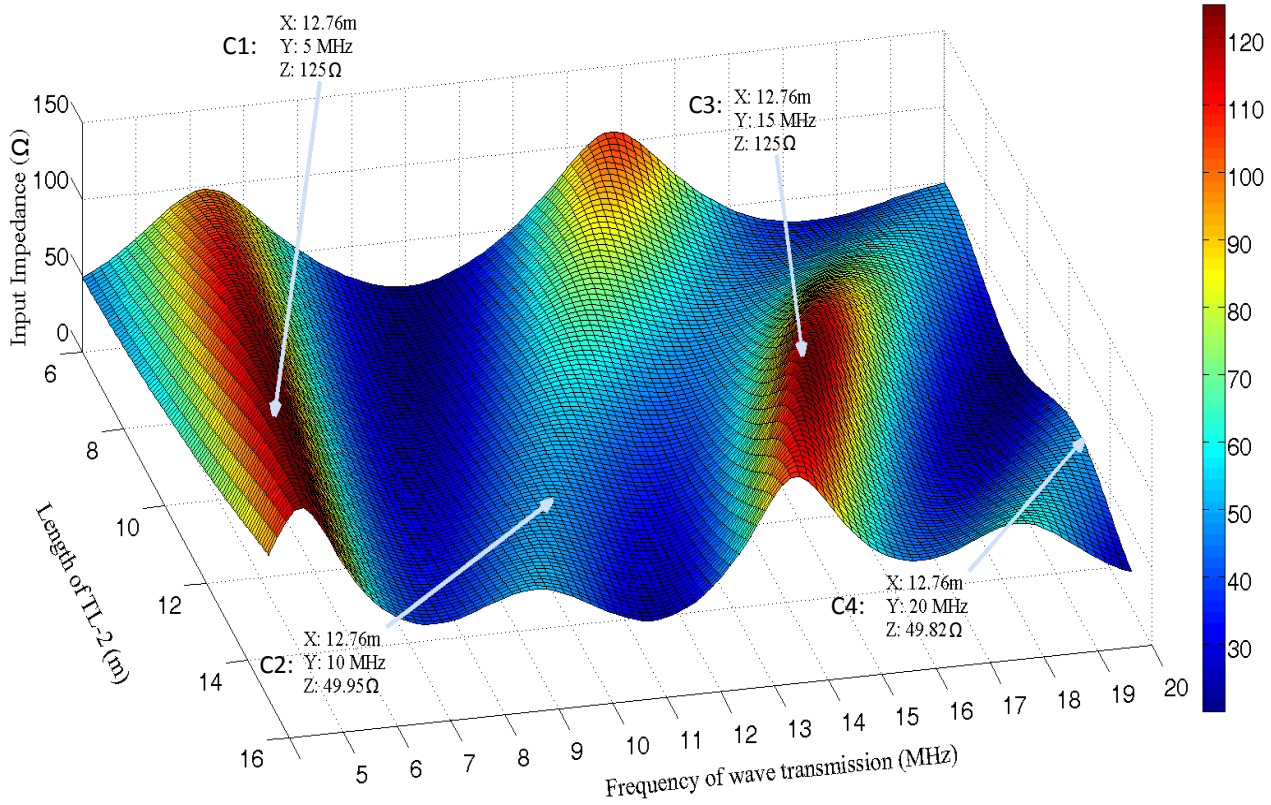

Figure 37. Variation in input impedance (marked with Z) with variation in frequency of wave transmission (marked with Y) and TL-2 length (marked with X) for a SIMO topology.

Figure 37 illustrates a simulated 3-D parametric variation in input impedance (marked with Z) with frequency of wave transmission (marked with Y) and TL-2 length (marked with X) for a SIMO topology as shown in Figure 16. The input impedances calculated by time domain plots in Figure 36 are captured by three points marked with C2, C3 and C4 in Figure 37.

3.4. HFDPS with MIMO topology

Next, for ascertaining the validity of (2.45) and (2.46) for power flow in a MIMO topology as shown in Figure 20, an experimental setup was developed. Table 3 displays the parameters used for the validation of MIMO topology.

Table 4. Parameters used for experimental validation of MIMO topology

Parameters	Values
Sources	Frequency (S_2:10 MHz, S_3: 20 MHz)
Loads	Impedance (Z_{L1}= 100 Ω , Z_{L2}= 100 Ω)
length	TL-1: 12.75 m, TL-2: 6.375m, TLF-1: 6.375m, TLF-2 : 6.375m

Condition (2.45) is satisfied by setting frequencies of wave transmissions or signal frequencies corresponding to S_2 and S_3 to be 10 MHz and 20 MHz, respectively. This ensures, following section 2.2.1 and in the absence of crosstalk, mitigation of noise in the transmitted power signals being fed to two 100 Ω loads through two coupled transmission lines each with a physical length of 12.75 m. Next, the impacts of variation in coupling coefficient (K) of the TL network and transmission-line-based band-stop filters on the validity of (2.46) is investigated. Figure 15 demonstrates the variation in the signal-to-interference-noise ratio (SINR) of voltage and current as a function of K. Due to coupling in the TL network, the crosstalk noise frequency for the path between S_2 and L_2 and S_3 and L_3 are found to be 20 MHz and 10 MHz, respectively. It is evident from Figure 38 that, the SINR increases as K is decreased because with progressively lower values of K, Z_{23} and Z_{32} in (2.46) approach infinity thereby further reducing the impact of crosstalk noise.

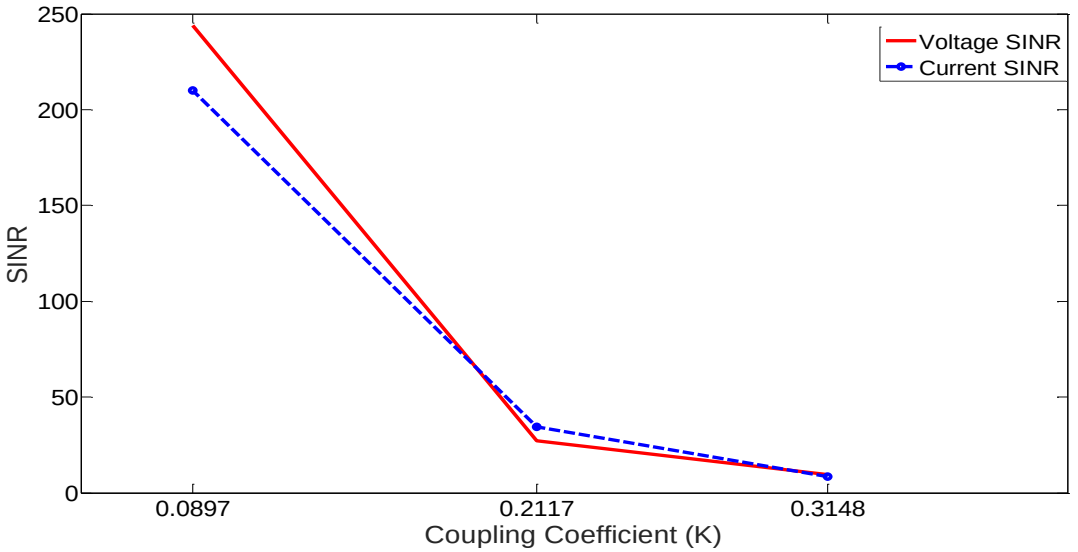

(a)

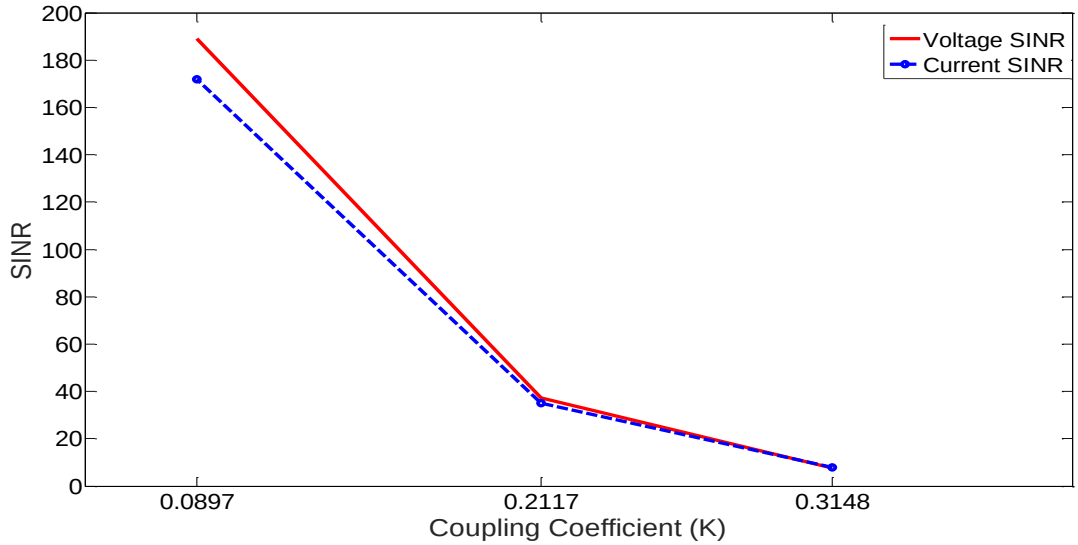

(b)

Figure 38. Variations in experimental SINRs of the voltage and current as a function of K. (a) At the input of TL-2 having fundamental component of 10 MHz with a 20 MHz noise frequency. (b) At the input of TL-3 having a fundamental component of 20 MHz with 10 MHz noise frequency.

To satisfy (2.46), we pursue an alternate approach by placing band-stop filters, tuned at band-stop frequencies of 20 MHz and 10 MHz, respectively, in the paths between S2 and L2 an S3 and L3. For simplicity, the band-stop filter was designed using transmission line, as outlined in

Appendix A. Figure 39 compares the variation in SINR for K = 0.3148 with and without the use of band-stop filters. The results show a significant improvement in SINR for both the current and voltage waveforms at the input of the TL-2 and TL-3. This is achieved by attaining very high values of Z_{23} and Z_{32} using properly tuned band-stop filters that mitigate the crosstalk signals.

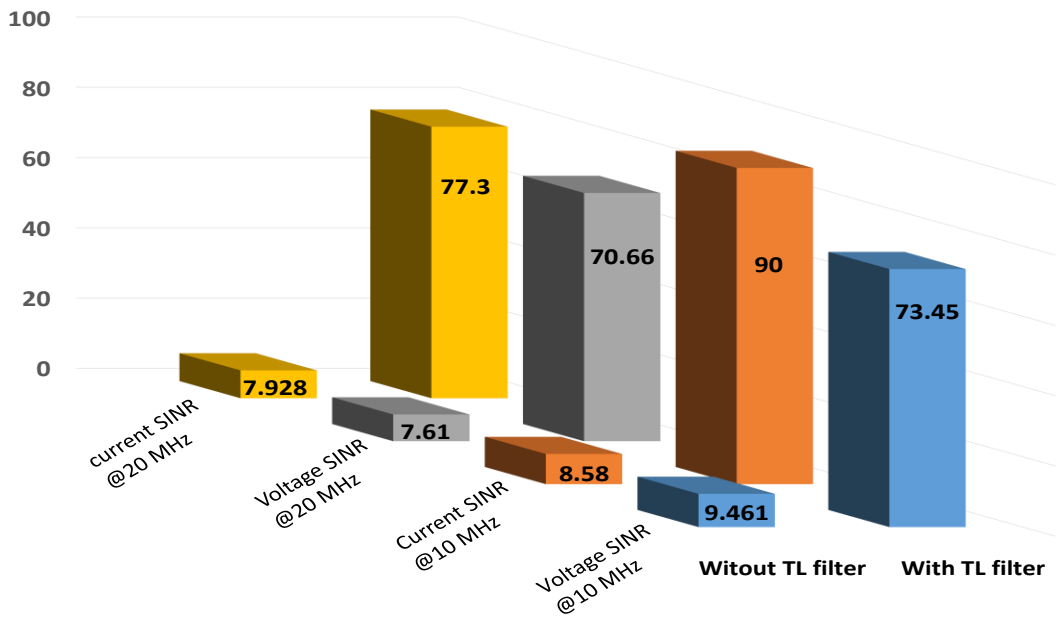

Figure 39. Comparison of experimentally-obtained SINRs with and without the band-stop filter for the MIMO topologies shown in Figures 21 and 24, respectively.

The frequency-dependent criteria outlined in chapter II of this Dissertation has been validated through frequency-domain and time-domain experimentation. In addition, its validation is extended further to SISO, SIMO and MIMO topologies. To ensure the signal integrity of the transmitted power signal in a SISO topology, frequency of wave transmission must satisfy (2.39c).

Finally, the impact of transmitting a periodic signal synthesized using plurality of frequencies in the presence of TL effects has been analyzed. Instead of transmitting a signal comprising only

one of these discrete frequency components, if a signal comprising of plurality of these discrete-frequency components is transmitted, then one can expect no signal-integrity issue in the power signal as well. Figure 40 shows the outcome of such a prediction using a bipolar square-wave signal (of 0.5 duty ratio) that has a fundamental frequency of 10 MHz and superharmonics that are multiples of 10 MHz yielding $V\ (t) = \sum \frac{4V_p}{(2M-1)\pi} \sin(2M-1)\omega t$, where V_p represents the peak voltage of the square wave and M represents consecutive positive integer with an initial value of 1.

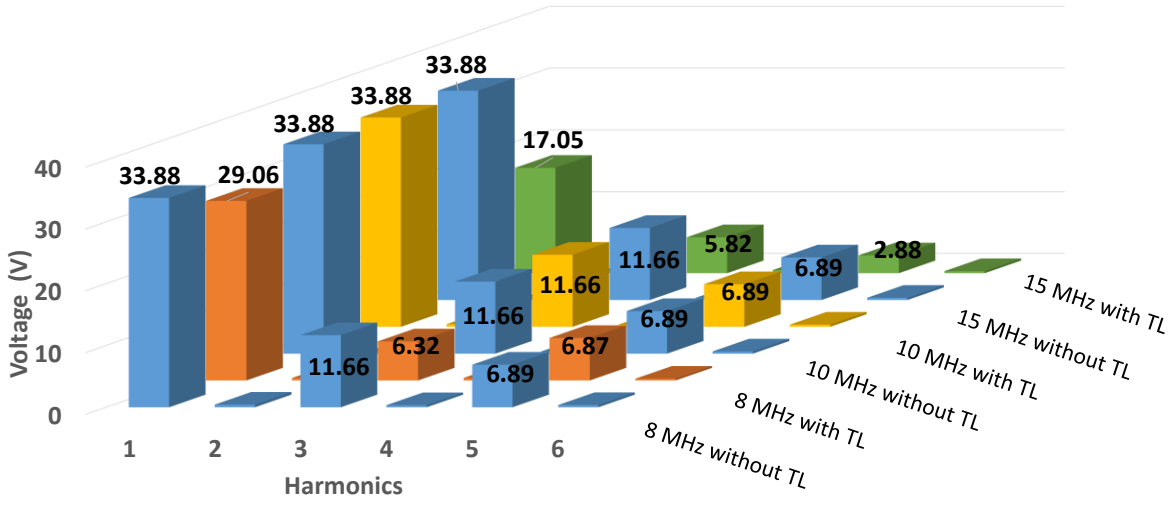

Figure 40. Experimental result showing comparison of harmonic-voltage components when a square wave is transmitted in the absence or presence of TL effect.

It is noted that, the 10 MHz frequency component and the superharmonics are chosen from a set that satisfy (10a). In Fig. 40, RMS voltage of each harmonic component at the source is plotted for two cases: one when the signal is sent through a TL network of length 12.75 m and the other when no TL network is used. It is apparent from Fig. 40 that, and as expected, for the case under consideration, the magnitudes of the harmonic components for these two cases do not show any

significant difference. However, when the two scenario-centric analyses were repeated for 8 MHz and 15 MHz base frequency of the bipolar square wave, a tangible difference was observed in the amplitudes of the base and superharmonic frequency components. This is because both 8 MHz and 15 MHz base frequency and their superharmonic components do not satisfy the impedance criterion (2.38a).

CONCLUSION

The maturity of a standalone high frequency power electronics has opened the possibility of HFDPS, which has the potential for delivering advantages including high power density, rapid power flow, high control bandwidth and reduced localized storage requirements. However, a HF PES brings forth the possibility of transmission-line effects that can affect the signal quality. Although, some researchers have demonstrated approaches to mitigate transmission-line effects by utilizing impedance matching networks, quarter wave transformers, filters and series or parallel stubs (L sections), others have employed active compensation or power factor correction techniques, thus ensuring power quality and signal integrity. While the former is limited where layout of the system can easily be altered by adjusting the length, latter leads to an increase in associated cost and complexity of the compensated system. This Dissertation provides a frequency-dependent criteria for systems terminated with passive linear loads, such that signal integrity is maintained under periodic condition in lieu of transmission-line effects. With regard to overall analysis, it is observed that, the frequency-dependent criteria remain same for SISO and SIMO topologies, while an additional analysis is required for MIMO topologies to reduce the prospects between power-transmission paths in TL network. Finally, the Dissertation illustrates a bipolar time-domain signal synthesized using discrete set of frequencies that individually satisfies frequency-dependent criteria for SISO topology also mitigate transmission-line effect.

FUTURE WORK

It was found that frequency-dependent criteria is applicable to the systems which are terminated with passive linear loads. The future work can be to identify its applicability to non-linear loads that encompass pulsating loads, power converters and dynamic loads. Also, the analysis done in the Dissertation employs sinusoidal signals for power transmission through transmission line. The future work can include the applicability of frequency-dependent criteria to wave shapes including square-waves, trapezoidal-waves or triangular-waves on SISO, SIMO and MIMO topologies. Also, how to minimize the crosstalk without employing transmission-line based band–stop filters in HFDPS connected in MIMO topology can be examined.

CITED LITERATURE

[1] Z. Liu, F. Wen, and G. Ledwich, "Potential benefits of distributed generators to power systems," in *2011 4th International Conference on Electric Utility Deregulation and Restructuring and Power Technologies (DRPT)*, 2011, pp. 1417–1423.

[2] R. Strzelecki and G. Benysek, "Power electronics in smart electrical energy networks," in *Power Systems*, 1st ed., vol. 34, Gdynia: Springer, 2008, pp. 175–200.

[3] M. Tahir and S. Maxumder, "Self-triggered Communication Enabled Control of Distributed Generation in Microgrids," *IEEE Trans. Ind. Informatics*, vol. 11, no. 2, pp. 1–1, 2015.

[4] A. Gupta, N. Kumar, and S. Mazumder, "High-Frequency Power Distribution in the Presence of Transmission-Line Effect."submitted for review in IEEE Trans. Power Electronics."

[5] R. M. Button, A. S. Brush, and R. C. Sundberg, "Development and testing of a 20 kHz component test bed," in *Proceedings of the 24th Intersociety Energy Conversion Engineering Conference*, 1989, pp. 605–610.

[6] P. K. Jain and M. C. Tanju, "A 20 kHz hybrid resonant power source for the space station," *IEEE Trans. Aerosp. Electron. Syst.*, vol. 25, no. 4, pp. 491–496, Jul. 1989.

[7] P. K. Sood and T. A. Lipo, "Power conversion distribution system using a high-frequency AC link," *IEEE Trans. Ind. Appl.*, vol. 24, no. 2, pp. 288–300, 1988.

[8] P. Jain, "A hybrid high frequency AC power distribution architecture for telecommunication systems," in *Proceedings of International Conference on Power Electronics, Drives and Energy Systems for Industrial Growth*, 1996, vol. 2, pp. 656–661.

[9] C. C. Antaloae, J. Marco, and N. D. Vaughan, "Feasibility of High-Frequency Alternating Current Power for Motor Auxiliary Loads in Vehicles," *IEEE Trans. Veh. Technol.*, vol. 60, no. 2, pp. 390–405, Feb. 2011.

[10] B. K. Bose and M. D. Kankam, "High frequency AC vs. DC distribution system for next generation hybrid electric vehicle," in *Proceedings of the 1996 IEEE IECON. 22nd International Conference on Industrial Electronics, Control, and Instrumentation*, 1996, vol. 2, pp. 706–712.

[11] S. Chakraborty, M. D. Weiss, and M. G. Simoes, "Distributed Intelligent Energy Management System for a Single-Phase High-Frequency AC Microgrid," *IEEE Trans. Ind. Electron.*, vol. 54, no. 1, pp. 97–109, Feb. 2007.

[12] S. Lourdes, S. Y. Ng, and P. C. K. Luk, "An alternative power grid - High frequency AC power distribution platforms," in *2009 IEEE 6th International Power Electronics and Motion Control Conference*, 2009, pp. 1949–1956.

CITED LITERATURE (continued)

[13] J. G. Kassakian and M. F. Schlecht, “High-frequency high-density converters for distributed power supply systems,” *Proc. IEEE*, vol. 76, no. 4, pp. 362–376, Apr. 1988.

[14] P. Jain, M. Pahlevaninezhad, S. Pan, and J. Drobnik, “A Review of High-Frequency Power Distribution Systems: For Space, Telecommunication, and Computer Applications,” *IEEE Trans. Power Electron.*, vol. 29, no. 8, pp. 3852–3863, Aug. 2014.

[15] H. Ohguchi, M. H. Ohsato, T. Shimizu, G. Kimura, and H. Takagi, “A high-frequency electronic ballast for HID lamps based on a λ/4-long distributed constant line,” *IEEE Trans. Power Electron.*, vol. 13, no. 6, pp. 1023–1029, 1998.

[16] T. Kawahara, T. Shimizu, M. Shioya, and G. Kimura, “High frequency power transmission by lumped constant circuit replaced distributed constant line,” in *15th Annual Conference of IEEE Industrial Electronics Society*, 1989, pp. 77–81.

[17] S. Sander, “Buck and Boost Converters With Transmission Lines,” *IEEE Trans. Power Electron.*, vol. 27, no. 9, pp. 4013–4020, Sep. 2012.

[18] P. A. Dalal, H. Y. Yang, and C. Q. Lee, “High frequency transmission line transformer for DC/DC converters,” in *Proceedings of PESC ’95 - Power Electronics Specialist Conference*, 1995, vol. 2, pp. 671–677.

[19] J. Kim and F. Bien, “Electric field coupling technique of wireless power transfer for electric vehicles,” in *IEEE 2013 Tencon - Spring*, 2013, pp. 267–271.

[20] F. A. Regier, “Impedance matching with a series transmission line section,” *Proc. IEEE*, vol. 59, no. 7, pp. 1133–1134, 1971.

[21] I. Takahashi and G. J. Su, “A 500 Hz power system-power converter and transmission lines,” in *Conference Record of the IEEE Industry Applications Society Annual Meeting*, 1989, pp. 988–995.

[22] A. Deutsch, G. V. Kopcsay, P. Restle, G. Katopis, W. D. Becker, H. Smith, P. W. Coteus, C. W. Surovic, B. J. Rubin, R. P. Dunne, T. Gallo, K. A. Jenkins, L. M. Terman, R. H. Dennard, G. A. Sai-Halasz, and D. R. Knebel, “When are transmission-line effects important for on-chip interconnections,” in *1997 Proceedings 47th Electronic Components and Technology Conference*, 1997, pp. 704–712.

[23] E. Persson, “Transient effects in application of PWM inverters to induction motors,” in *Conference Record of 1991 Annual Pulp and Paper Industry Technical Conference*, 1991, pp. 228–233.

CITED LITERATURE (continued)

[24] D. B. Hyypio, “Effects of risetime and cable length on motor insulation degradation resulting from operation on PWM voltage source inverters,” in *1997 IEEE International Electric Machines and Drives Conference Record*, 1997, pp. TC3/2.1–TC3/2.3.

[25] P. Brogan, W. Phang, R. Yacamini, and A. Scott, “Variable speed drives for remote downhole pump applications,” *Power Eng. J.*, vol. 14, no. 1, pp. 29–36, Feb. 2000.

[26] P. Andrew and G. Durgin, “Transient Signals on Transmission Lines:An Introduction to Non-Ideal Effects and Signal Integrity Issues in Electrical Systems,” 1st ed., 2009, pp. 11–21.

[27] D. M Pozar, “Microwave Engineering, 3rd,” in *John Wiley and Sons Inc.*, 2005, p. 728.

VITA

NAME: NIKHIL KUMAR

EDUCATION : B.E., Electrical Engineering, Delhi College of engineering, Delhi, India, 2011

M.S., Electrical and Computer Engineering, University of Illinois at Chicago, Chicago, Illinois, 2015

EXPERIENCE : Executive Engineer, Mumbai Monorail Project, Larsen & Toubro, Mumbai, India, Summer 2011- Summer 2013

Teaching Assistant, University of Illinois at Chicago, Chicago; Electromechanical energy Conversion (ECE 458), Analysis and Design of Power electronics (ECE 445), Linear Control systems (ECE 550), Electronics-I (ECE 340)

PUBLICATION:

A. Gupta, N. Kumar, and S. Mazumder, "High-Frequency Power Distribution in the Presence of Transmission-Line Effect."submitted for review in IEEE Trans. Power Electronics."

A. Gupta, N. Kumar and S. Mazumder, "Frequency-Dependent Criterion for Mitigation of Transmission-Line Effects in a High-frequency Distributed Power Systems" to be presented at Energy Conversion congress & Expo (ECCE), Montreal, Canada, 2015.